Geoscience Frontiers 11 (2020) 745–763

Contents lists available at ScienceDirect

Geoscience Frontiers

journal homepage: www.elsevier.com/locate/gsf

Research Paper

Garnet fractionation, progressive melt loss and bulk composition variations in anatectic metabasites: Complications for interpreting the geodynamic significance of TTGs

Jillian Kendrick *, Chris Yakymchuk

Department of Earth and Environmental Sciences, University of Waterloo, Waterloo, Ontario, N2L 3G1, Canada

ARTICLE INFO

Handling Editor: Richard M Palin

Keywords:
Archean
Anatexis
Trace element
Phase equilibrium modelling
Tectonics

ABSTRACT

Tonalite-trondhjemite-granodiorite (TTG) suites constitute a large proportion of the Archean geological record; however, the geodynamic processes that generated them, and Archean continental crust in general, remain a subject of debate. The concentrations and ratios of Sr, Y, La, Yb, Nb, and Ta in TTGs are commonly used to determine the depth of melting of their metabasic sources. The trace element composition of melt produced by metabasic source rocks during anatexis is strongly affected by the presence and abundance of pressure-sensitive minerals, such as plagioclase (Sr-bearing), garnet (Y- and HREE-bearing), and rutile (Nb- and Ta-bearing). Elevated Sr/Y and La/Yb ratios and low concentrations of Nb and Ta in TTGs are generally considered to indicate melting at high pressures (≥2.0 GPa). The depth of melting is a key factor in determining the origin of TTGs as this provides critical information on the tectonic setting of their generation. We use phase equilibrium and trace element modelling to explore the effects of three potential influences on TTG trace element compositions: fractionation of trace elements into peritectic garnet cores, progressive melt loss from the source, and source bulk composition. We model three different compositions of Archean basalts along thermal gradients of 500 °C/GPa, 750 °C/GPa, and 1000 °C/GPa. The models produce major and trace element melt compositions that are generally consistent with measured compositions of TTGs. Although Sr/Y, La/Yb, Nb, and Ta exhibit pressure-dependent behaviour, other factors also affect these values. Garnet fractionation causes Sr/Y and La/Yb to reach much greater values and in this scenario, the values also increase with increasing temperature. Source bulk composition has an effect in all scenarios and most strongly influences La/Yb, Nb, and Ta. Overall, these results show that Sr/Y, La/Yb, Nb, and Ta can reach values generally considered to be indicative of high pressure melting at a range of P–T conditions including $P < 2.0$ GPa. Consequently, trace element compositions of TTGs alone may provide a misleading impression of the depth of melting of metabasites and the geodynamic environment of Archean crustal growth and reworking.

1. Introduction

Tonalite-trondhjemite-granodiorite suites, or TTGs, volumetrically dominate Archean cratons, but the geodynamic setting in which they formed remains contentious (Martin et al., 2005; Moyen, 2011; Bédard, 2018; Condie, 2018; Moyen and Laurent, 2018). It is generally accepted that TTGs are generated from the partial melting of hydrated metabasites (Rapp et al., 1991; Moyen and Martin, 2012; Nagel et al., 2012; Martin et al., 2014; Moyen and Laurent, 2018). Concentrations and ratios of specific trace elements in TTGs are commonly used to infer the depth of melting of their metabasic sources, and this is used to infer the tectonic processes that led to their genesis (Martin et al., 2005; Moyen and Stevens, 2006; Moyen and Martin, 2012). This has led to several interpretations for the genesis of TTGs that include partial melting of subducted oceanic crust (Drummond and Defant, 1990), melting of thickened crust in an arc-like setting (Nagel et al., 2012), and melting at the base of oceanic plateaux (Bédard, 2006). The depth of partial melting is a key distinguishing factor for these different settings and identifying evidence in TTGs for these processes has important implications for the origin and evolution of Archean cratons.

During partial melting of metabasites, a strong control on the trace element concentrations and ratios in equilibrated melt is the presence

* Corresponding author.
E-mail address: jlkendrick@uwaterloo.ca (J. Kendrick).
Peer-review under responsibility of China University of Geosciences (Beijing).

https://doi.org/10.1016/j.gsf.2019.12.001
Received 3 July 2019; Received in revised form 30 September 2019; Accepted 5 December 2019
Available online 18 December 2019
1674-9871/© 2019 China University of Geosciences (Beijing) and Peking University. Production and hosting by Elsevier B.V. This is an open access article under the CC BY-NC-ND license (http://creativecommons.org/licenses/by-nc-nd/4.0/).

and abundance of garnet, plagioclase, and rutile (Defant and Drummond, 1990). These minerals have broadly pressure-sensitive stability fields in metabasites. In general, garnet is stable at high pressures and contains high concentrations of HREEs and Y, rutile is also stable at high pressures and is rich in Nb and Ta, and plagioclase is stable at relatively low pressures and is enriched in Sr. Regardless of the geodynamic processes involved, the presence (or absence) and abundance of these minerals in the source during melting is expected to impart a distinct trace element signature to the extracted melt that ultimately forms TTGs. Assuming all phases are in thermodynamic equilibrium, partial melting at high pressures is expected to proceed with garnet and rutile in the residue; these minerals preferentially partition the HREEs, Y, Nb, and Ta and this leaves the melt relatively depleted in these elements. By contrast, melting at low pressures in the plagioclase stability field will cause the melt to be depleted in Sr, but relatively enriched in HREEs, Y, Nb, and Ta due to the absence of garnet and rutile. Thus, the Sr/Y and La/Yb ratios of TTGs are commonly used as proxies of depth of melting (Moyen and Stevens, 2006; Moyen and Martin, 2012), as these ratios should increase with increasing pressure of melting as the metabasic source transitions from the plagioclase stability field to the garnet stability field. The depletion of Nb and Ta in TTGs is used as an additional indicator of high-pressure melting based on the stability of rutile. Based on Sr, Y, La, Yb, Nb, and Ta systematics in natural samples, Moyen (2011) defined three groups of TTGs linked to depth of melting: the low pressure group, produced at 1.0–1.2 GPa by a garnet-free, plagioclase-bearing source; the medium pressure group, corresponding to approximately 1.5 GPa with garnet, some or no rutile, and no plagioclase in the source; and the high pressure group, produced at $\geq$ 2.0 GPa in the presence of garnet and rutile without plagioclase. The different pressures of source melting can be linked to the conceptual geodynamic models of TTG generation, and this is crucial for understanding the formation, reworking, and stabilisation of Archean cratons.

Recent advances in thermodynamic modelling of phase assemblages in anatectic metabasites (e.g. Palin et al., 2016b) coupled with trace element modelling (e.g. Johnson et al., 2017; Janousek and Moyen, 2019) present an opportunity to forward model the major and trace element compositions of melt generated in metabasites at a range of *P–T* conditions and for various petrological scenarios. Although this technique has been used to model TTG trace element compositions assuming closed-system behaviour (Nagel et al., 2012; Johnson et al., 2017; Gardiner et al., 2018), previous studies have not investigated the various petrological factors that may influence Sr, Y, La, Yb, Nb, and Ta systematics in natural systems. In particular, open-system processes can modify the stability and modal proportions of minerals during high temperature metamorphism and anatexis (White et al., 2004; Yakymchuk and Brown, 2014, 2019; Mayne et al., 2016, 2019; Stuck and Diener, 2018; Villaros et al., 2018), and may affect trace element partitioning. Furthermore, fractionation of key trace elements into growing porphyroblasts such as garnet can limit their availability to the melt (e.g. Otamendi et al., 2002). In addition, mafic sources may have variable trace element compositions prior to melting, and differences in major element composition may cause garnet, plagioclase, and rutile to be produced at different *P–T* conditions and in different proportions, which has implications for linking trace elements of TTGs to depth of melting and their geodynamic settings.

Here we use forward modelling of three different mafic source compositions to demonstrate the effects of open-system melting (i.e. progressive melt loss), fractionation of trace elements into garnet, and source bulk composition on the trace element composition of TTGs. We assess the impact of these factors on the elements typically used to infer the depth of melting: Sr, Y, La, Yb, Nb, and Ta. Trace element concentrations were calculated for melt produced in each scenario for each bulk composition at a range of *P–T* conditions. The results of the modelling are evaluated in the context of natural TTG data (Moyen, 2011; Johnson et al., 2019) and the compositional groups defined by Moyen (2011). Overall, our results suggest that the Sr/Y, La/Yb, Nb, and Ta parameters of the melt may not have a simple relationship with pressure, and these geochemical characteristics alone may give a misleading impression of the depth of melting and the nature of geodynamic processes accompanying TTG generation in the Archean Eon.

2. Methodology

2.1. Selection of source compositions

Geochemical studies of TTGs and melting experiments have indicated that hydrated mafic crust is the most compatible source for TTGs (Jahn et al., 1981; Martin, 1986; Rapp et al., 1991; Rapp and Watson, 1995; Springer and Seck, 1997; Qian and Hermann, 2013) and LILE and LREE enrichment may be required (Martin et al., 2014); however, the chemical compositions of potential Archean basaltic sources are variable. Three recent phase equilibrium modelling studies used different approaches to select potential TTG sources. Nagel et al. (2012) chose to model melting of a modern mid-ocean ridge basalt (MORB) and an Eoarchean tholeiitic basalt from the Isua Supracrustal Belt in Greenland to determine the depth of melting required to reproduce the trace element compositions of Eoarchean TTGs. The Eoarchean tholeiite composition produced melts with the greatest similarity to Eoarchean TTGs, with the best fit corresponding to melts produced at 1.0 GPa and 1.4 GPa. Palin et al. (2016b) chose an average LILE- and LREE-enriched Archean tholeiite (EAT, Condie, 1981, Table 1) and an average LILE- and LREE-depleted Archean tholeiite (DAT, Condie, 1981, Table 1) and modelled the major element compositions of melts produced at varying *P–T* conditions in closed and open system scenarios. The modelling produced melt major element compositions consistent with those of natural TTGs at *P–T* conditions of 800–950 °C and ~1.0–1.8 GPa. Johnson et al. (2017) focused on modelling the major and trace element compositions of Palaeoarchean TTGs from the Pilbara Craton in Western Australia, for which a source basalt rich in incompatible trace elements has been proposed (Coucal basalts; Smithies et al., 2009). The compositions of the TTGs were reproduced by the model for melting at *P–T* conditions of 850–900 °C and <1.3 GPa. Therefore, various potential sources for TTGs have been modelled, and are in each case selected to suit the scope and purpose of the study.

For the purposes of this study, we chose to build upon the work of Palin et al. (2016b) and use two average Archean basalt compositions to evaluate the general effects of melt loss, garnet fractionation, and source bulk composition on the trace element composition of TTGs, but we acknowledge that understanding specific TTGs suites may require modelling of associated parental basalts (e.g. Johnson et al., 2017). To determine if EAT and DAT (Condie, 1981; Palin et al., 2016b) represent average Archean basalts based on major element composition, we compared them to a compilation of whole rock geochemical data from 1435 Archean basalts (Fig. 1; Supplementary Table 1) created using the sources cited in the basalt and komatiite geochemical database of Condie et al. (2016). Our criteria for selecting compositions to add to the compilation differ from those of Condie et al. (2016), who only included basalts with MgO concentrations of 7–17 wt.%. Given that the average Coucal basalt composition modelled by Johnson et al. (2017) contained only 3.80 wt.% MgO, we elected to include all basalts below 17 wt.% MgO (in an anhydrous system). Additionally, the compositions were screened based on SiO_2 content ($\leq$60 wt.% on an anhydrous basis) and any rocks stated to be of intrusive origin were not included. Plots of SiO_2 vs. MgO and Al_2O_3 vs. CaO (Fig. 1) produced from our database indicate that the major element compositions of EAT and DAT are typical of Archean basalts. Johnson et al. (2017) found that the low MgO content of the Coucal basalt composition allowed for stabilisation of garnet at relatively low pressures. However, other workers have suggested that MgO-rich basalts were more common in the Archean and are underrepresented in the currently preserved Archean geological record (e.g. Palin and Dyck, 2018). Given the importance of garnet as a reservoir for Y and HREEs, the MgO content of the mafic source may be an important factor

Table 1
Archean basalt compositions (oxide in wt.%, trace elements in ppm) selected for modelling from Condie (1981; EAT and DAT) and Szilas et al. (2013; MAB).

	SiO_2	TiO_2	Al_2O_3	FeO	Fe_2O_3	MnO	MgO	CaO	Na_2O	K_2O	Sr	Y	La	Yb	Nb	Ta
EAT	50.85	1.53	15.62	9.42	2.88	0.18	7.01	9.03	2.77	0.71	190	30	13	2.2	12.8	0.78
DAT	50.58	0.95	15.62	9.33	1.64	0.22	7.59	11.69	2.17	0.22	100	20	3.6	1.9	5	0.29
MAB	50.14	0.49	11.90	0.00	11.98[a]	0.19	14.27	9.29	1.36	0.33	78.9	12.6	2.7	1.24	0.8	0.1

[a] Total Fe reported as Fe_2O_3. DAT = depleted Archean tholeiite, EAT = enriched Archean tholeiite, MAB = MgO-rich Archean basalt.

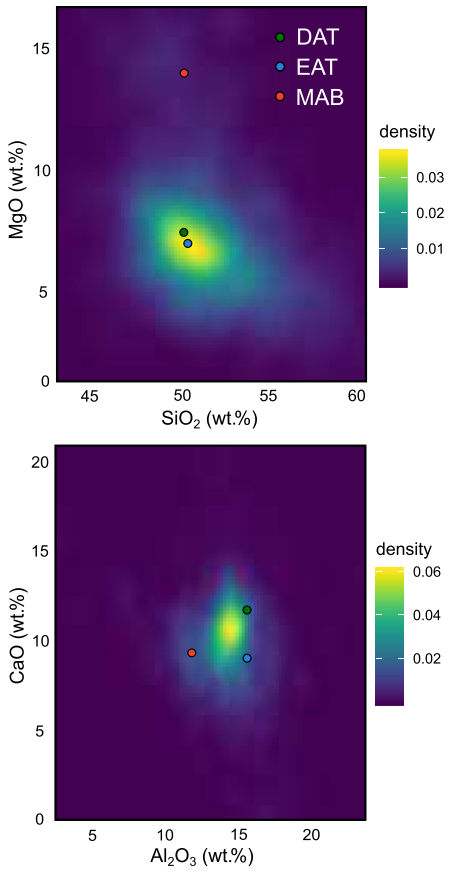


Fig. 1. Two-dimensional kernel density estimation of SiO_2 vs. MgO and Al_2O_3 vs. CaO from whole rock geochemical data in the Archean basalt compilation provided in Supplementary Table 1. The plots were generated using the stat_density_2d function in the ggplot2 package (Wickham, 2011) available for the R programming language. DAT = depleted Archean tholeiite, EAT = enriched Archean tholeiite, MAB = MgO-rich Archean basalt.

in melt trace element composition. To test this, we additionally selected a composition from a population of MgO-rich basalts (Fig. 1), which will be referred to here as the MgO-rich Archean basalt (MAB). The MAB composition, including major and relevant trace elements, is from a greenschist sample from the Tartoq Group supracrustal rocks in south-western Greenland (sample 510878 of Szilas et al., 2013, Table 1).

The elements selected for melt trace element modelling were Sr, Y, La, Yb, Nb, and Ta as these are commonly linked to the depth of partial melting. For the three basalt compositions investigated, Sr, Y, La, and Yb concentrations were included in the source data (Condie, 1981; Szilas et al., 2013), and Nb and Ta were reported only for MAB (Szilas et al., 2013). We assigned to EAT the Nb and Ta of the average Coucal basalt (as reported by Johnson et al., 2017), as this suite of basalts shows trace element enrichment similar to EAT. This Nb concentration is relatively high, as it falls within the top 1% of Nb concentrations in a compilation of Archean basalt compositions from Australia (Smithies et al., 2018). However, suites of Nb-enriched basalts have been recognized in several Archean greenstone belts in the Superior province (Hollings and Kerrich, 2000; Wyman et al., 2000; Polat and Kerrich, 2001; Hollings, 2002), suggesting that basalts with high Nb concentrations are not a localized feature. Therefore, the concentration selected for EAT is considered here to be representative of a high-Nb endmember. For DAT, a moderate Nb concentration was chosen to differentiate it from EAT and the Nb-poor MAB. The Ta value for DAT was calculated based on the established Nb/Ta value of the primitive mantle (17.5 ± 2; Green, 1995). The trace element compositions are specified in Table 1 for the three modelled compositions.

2.2. Phase equilibrium modelling

Phase equilibrium modelling was done in the Na_2O–CaO–K_2O–FeO–MgO–Al_2O_3–SiO_2–H_2O–TiO_2–Fe_2O_3 (NCKFMASHTO) chemical system using Thermocalc version 3.45 (Powell and Holland, 1988) and the internally consistent thermodynamic dataset of Holland and Powell (2011; updated version ds62). The activity–composition (a–x) models used are as follows: tonalitic melt, amphibole, clinopyroxene (Green et al., 2016), orthopyroxene, garnet, biotite, muscovite, ilmenite (White et al., 2014), K-feldspar, plagioclase (Holland and Powell, 2003), and epidote (Holland and Powell, 2011). Rutile, quartz, titanite, and aqueous fluid (H_2O) were modelled as pure end members.

For each bulk composition, phase assemblages were calculated from the solidus to 1050 °C and between 0.4 GPa and 2.2 GPa. Also, phase proportions and compositions were extracted from Thermocalc across a grid at intervals of 25 °C and 0.1 GPa. For these calculations, the bulk H_2O contents of DAT, EAT, and MAB were reduced to minimally saturate melt in H_2O at the solidus at 1.2 GPa (Table 2). This was done because any free H_2O in suprasolidus rocks would be expected to partition into the melt (White and Powell, 2002; White et al., 2005). As FeO and Fe_2O_3 are not differentiated for MAB, an O value was assigned assuming a Fe^{2+}/Fe^{3+} ratio of 10. Additionally, phase proportion and composition data were collected along three P–T gradients for each bulk composition, 500 °C/GPa, 750 °C/GPa, and 1000 °C/GPa, which are considered to be plausible apparent geothermal gradients for Archean crust based on peak P–T estimates from Archean metamorphic rocks (Brown and Johnson, 2018). The 1000 °C/GPa thermal gradient was chosen for our modelling as a high dT/dP endmember based on the compilation of Brown and Johnson (2018), whereas 500 °C/GPa is the lowest dT/dP gradient recorded in Archean rocks in the compilation. These gradients are considered apparent thermal gradients and are simplified compared to natural P–T paths, which cannot typically be represented by a single gradient and may involve more complex prograde evolutions. For each of these P–T gradients, the H_2O contents of the bulk compositions were adjusted to just saturate melt in H_2O at the P–T conditions where the gradient intersects the solidus (Table 2). The data extracted from Thermocalc were converted to weight fractions and then coupled with published partition coefficients (from Bédard, 2006) for various trace elements in metabasites to calculate the trace element composition of the melt (i.e. TTGs) and residue using a batch melting model (e.g. Presnall, 1969; Shaw, 1970; Hanson, 1978). These calculations represent a scenario where the composition of the system remains constant and there is equilibrium of major and trace elements among all phases. This closed system behaviour is considered here as a baseline scenario, and additional modelling was undertaken to simulate two open system scenarios: loss of anatectic melt and fractionation of elements into garnet porphyroblasts.

Table 2
Compositions used in Thermocalc models (mol%).

	H_2O	SiO_2	Al_2O_3	CaO	MgO	FeO	K_2O	Na_2O	TiO_2	O	
DAT	6.10	49.36	9.89	12.22	11.04	8.82	0.14	2.05	0.70	0.60	sat 12 kbar
	5.29	49.30	9.88	12.21	11.03	8.81	0.14	2.05	0.70	0.60	sat 500 °C/GPa
	5.23	49.33	9.89	12.21	11.03	8.82	0.14	2.05	0.70	0.60	sat 750 °C/GPa
	4.53	49.70	9.96	12.30	11.12	8.88	0.14	2.06	0.70	0.60	sat 1000 °C/GPa
EAT	6.83	49.69	8.99	9.21	10.21	9.81	0.44	2.63	1.13	1.06	sat 12 kbar
	5.87	50.20	9.08	9.31	10.31	9.92	0.45	2.66	1.14	1.07	sat 500 °C/GPa
	5.11	50.61	9.16	9.38	10.39	10.00	0.45	2.68	1.15	1.08	sat 750 °C/GPa
	4.82	50.76	9.19	9.41	10.43	10.03	0.45	2.69	1.15	1.08	sat 1000 °C/GPa
MAB	5.80	49.72	6.96	9.87	21.10	4.47	0.22	1.30	0.37	0.23	sat 12 kbar
	5.56	49.84	6.97	9.89	21.15	4.48	0.22	1.30	0.37	0.23	sat 500 °C/GPa
	5.82	49.72	6.96	9.87	21.10	4.47	0.22	1.30	0.37	0.23	sat 750 °C/GPa
	5.83	49.72	6.96	9.87	21.10	4.47	0.22	1.30	0.37	0.23	sat 1000 °C/GPa

DAT = depleted Archean tholeiite, EAT = enriched Archean tholeiite, MAB = MgO-rich Archean basalt.

2.2.1. Open system behaviour

2.2.1.1. Melt loss. Loss of anatectic melt from suprasolidus rocks during prograde metamorphism is considered to be a common process, given that these rocks typically preserve peak metamorphic assemblages with minimal evidence of retrogression (White and Powell, 2002). This scenario was simulated by removing 6 mol% melt (approximately equivalent to 6 vol% on a one-oxide basis) in pulses along each *P–T* gradient when a proportion of 7 mol% melt was reached (cf. Yakymchuk and Brown, 2014), which approximates the melt connectivity threshold of Rosenberg and Handy (2005). This leaves 1 mol% melt in the system, which is consistent with the presence of melt pseudomorphs in some anatectic metamorphic rocks (e.g. Holness and Sawyer, 2008). The bulk compositions of major and trace elements in the system were adjusted based on the extraction of melt with equilibrium concentrations at the 7 mol% threshold.

2.2.1.2. Garnet fractionation. The preservation of major and trace element zonation in garnet porphyroblasts is a well-documented feature (e.g. Spear and Kohn, 1996; Pyle and Spear, 1999) that provides strong evidence for sequestration of these elements during garnet growth. As garnet is an important reservoir for HREEs and Y in metabasites, garnet fractionation could have a significant impact on the availability of these elements to anatectic melt. In addition, the low diffusivity of the HREE and Y in garnet relative to divalent cations (e.g. Fe, Mg; Carlson, 2012) hinders diffusional equilibration of these elements due to thermally-activated volume diffusion. Garnet fractionation was modelled by removing garnet along the *P–T* gradients in increments of 4.5 mol% when 5 mol% was reached. This simulates continuous segregation of garnet cores from the equilibrium assemblage of the rock, leaving a thin reactive rim comprising a ~10 mol% fraction of the garnet, which is equivalent to a ~30 μm-thick rim for a garnet crystal with a diameter of ~2 mm and ~170 μm for a ~10 mm diameter crystal. In other forward models of garnet growth, this reactive rim is < 10 μm (Gaidies et al., 2008) or considered to be negligible (e.g. Evans, 2004), but we include a reactive rim here given the high temperatures and presence of melt in our models. The major and trace elements associated with the 4.5 mol% of garnet sequestered from the system were removed from the modelled bulk compositions at each step, and the proportions of all residue phases were renormalized to a total of 1.

3. Results

3.1. P–T pseudosections

The *P–T* pseudosections produced for EAT (see also Palin et al., 2016b) and DAT have similar overall topologies, with modelled solidus temperatures ranging from approximately 625–725 °C; MAB shows distinct differences from the others, with a solidus at approximately 750 °C with a steep d*T*/d*P* (Fig. 2). Hornblende is predicted to be stable across a large portion of the three diagrams and is exhausted at 850–950 °C above 1.2–1.4 GPa. Similarly, quartz is stable at the solidus in all three diagrams, and is exhausted at temperatures as low as 800 °C at low *P*, but may persist up to 1000 °C at high *P*. Both clinopyroxene and orthopyroxene are predicted to be stable for all three bulk compositions, although their stability fields differ. Clinopyroxene is stable across the entire diagram for DAT, but for EAT and MAB, clinopyroxene is absent below 1.3 GPa and 750 °C and 1.9 GPa and 850 °C respectively. For EAT and DAT, orthopyroxene is restricted to pressures of ≤1.1 GPa at temperatures above 800–900 °C. For MAB, orthopyroxene is predicted to be stable at similar temperatures but persists up to at least 2.2 GPa.

The *P–T* stability fields of each of the trace element reservoirs, garnet, rutile, and plagioclase, are comparable for EAT and DAT, and slightly different for MAB (Fig. 3). Garnet is predicted to be stable at pressures as low as 0.8 GPa for DAT, 0.9 GPa for EAT, and 1.1 GPa for MAB at approximately 900 °C (Fig. 3a–c); however, at temperatures close to the solidus, the lower pressure limit of garnet stability increases to 1.2 GPa for DAT and 1.4 GPa for EAT and MAB. At similar *P–T* conditions, the weight proportions of garnet predicted for DAT are approximately 5 wt.% higher than those of EAT and 15–30 wt.% higher than those of MAB. Plagioclase is stable up to 1.9 GPa for EAT and 1.8 GPa for DAT, and this maximum pressure corresponds to 850 °C–900 °C (Fig. 3d and e). With decreasing or increasing temperature from this point, the upper pressure limit of plagioclase stability decreases to ~1.0 GPa at the lowest. The model for DAT predicts greater proportions of plagioclase than those of EAT, particularly at lower pressures, where the DAT composition may have up to 10 wt.% more plagioclase than the EAT composition. For MAB, the maximum pressure of the plagioclase stability field is 1.2 GPa at temperatures above 950 °C and decreases to 0.5 GPa at the solidus at 750 °C (Fig. 3f). The amount of plagioclase predicted for MAB is typically 10–15 wt.% less than that of DAT at similar *P–T* conditions. The low pressure limit of the rutile stability field is at 0.9 GPa for DAT and 1.0 GPa for EAT from approximately 900 °C to 1050 °C, and at lower temperatures the field becomes restricted to pressures above 1.5 GPa–1.6 GPa (Fig. 3g and h). The model for MAB predicts the presence of rutile above 1.6 GPa to almost 1.8 GPa below 900 °C (Fig. 3i), and differs significantly from DAT and EAT above 900 °C, where rutile is expected to be stable to ≤0.4 GPa. At high *P–T*, the model predicts that EAT will have approximately 1.5 times more rutile than DAT and 3 times more than MAB.

3.2. P–T gradients

Assemblages and weight fractions of each phase were calculated along three *P–T* gradients for each bulk composition and for each of the three modelled scenarios: closed system, melt loss, and garnet fractionation. Again, these gradients are intended to show simplified *P–T* paths

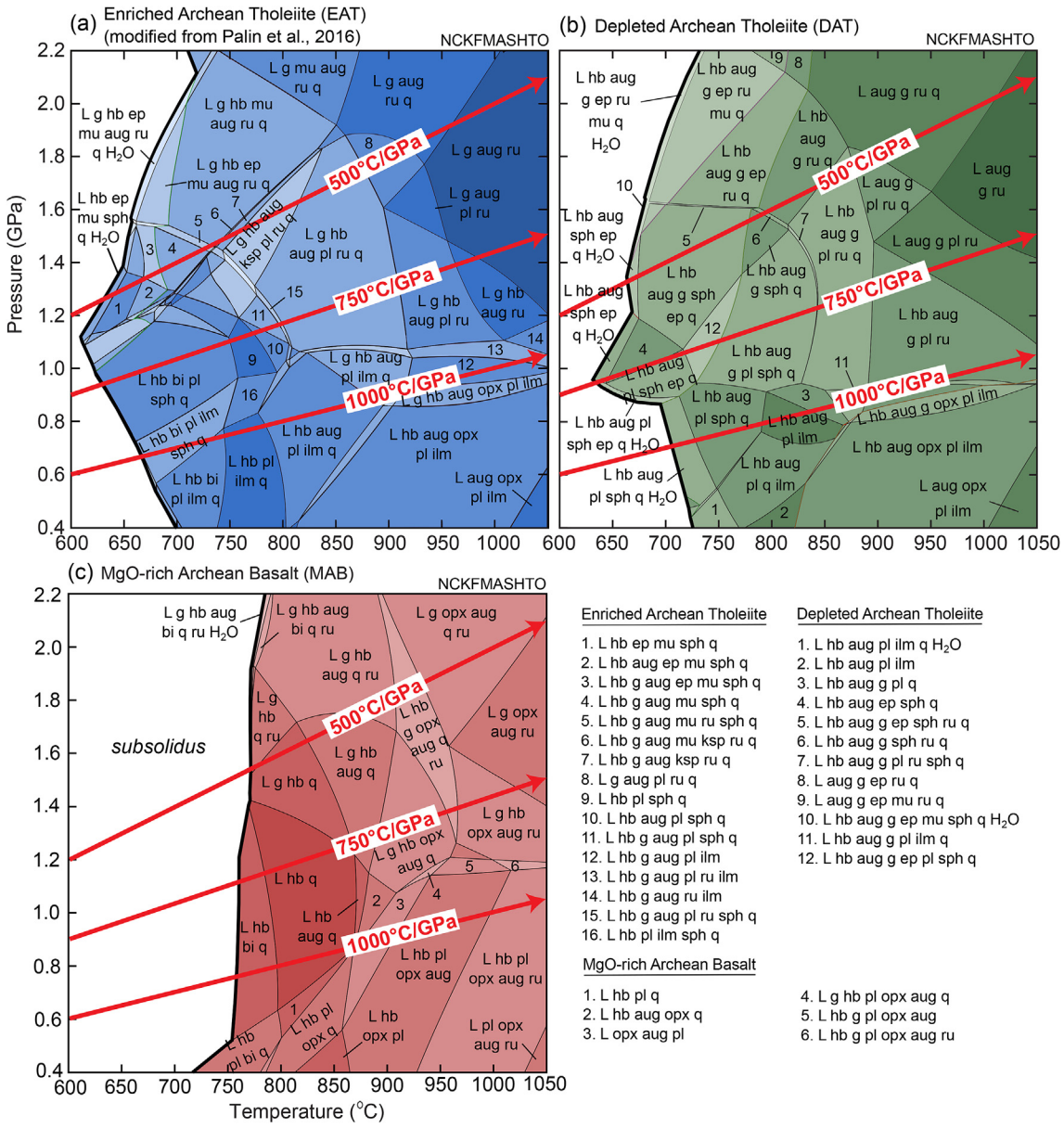


Fig. 2. *P–T* pseudosections for each of the modelled basalt compositions, the diagram for EAT has been modified from Palin et al. (2016b). The concentration of H_2O in each composition was selected to stabilize a minimal amount of free H_2O at the solidus at 1.2 GPa (Table 2). Phase abbreviations after Holland and Powell (2011).

up to peak metamorphic conditions recorded by Archean rocks (e.g. Brown and Johnson, 2018). The results from DAT are shown as an example (Fig. 4), as the same general trends are present for EAT and MAB (Supplementary Fig. 1). For comparison, see also Palin et al. (2016b), where phase proportions for EAT and DAT were previously calculated for isobaric heating paths.

Along the 500 °C/GPa gradient in the closed system scenario, the stable assemblage at the solidus is dominated by hornblende and quartz, with small amounts of clinopyroxene, garnet, and other minerals that are bulk composition-dependent (epidote, titanite, or muscovite). With increasing *P* and *T*, hornblende and quartz proportions decrease as garnet, clinopyroxene, and melt increase, and for DAT and EAT, plagioclase joins the modelled assemblage at ~800 °C. Rutile also becomes stable at this stage, at *P–T* conditions that vary with bulk composition. Near 900 °C and 1.8 GPa (925 °C and 1.85 GPa for MAB), hornblende is expected to be exhausted. At *P–T* conditions above hornblende out, changes in mineral proportions are relatively gradual, with quartz and plagioclase decreasing until plagioclase is exhausted, and garnet and clinopyroxene show little to no change in their modal proportions. Between 1000 °C and 1050 °C and 2.0 GPa and 2.1 GPa, quartz proportions reach zero, leaving an assemblage of garnet, clinopyroxene, rutile, and melt (and orthopyroxene for MAB). Proportions of melt continue to increase with clinopyroxene or garnet either increasing or decreasing slightly, depending on bulk composition; rutile proportions increase gradually for all compositions.

The mineral assemblages and trends in mineral proportions predicted along the 750 °C/GPa gradient in the closed system scenario are broadly similar to those of the 500 °C/GPa gradient. The major differences, for all bulk compositions, is garnet and rutile production at relatively higher *P–T*, the exhaustion of quartz before hornblende, and the presence of biotite up to ~800 °C in EAT (Supplementary Fig. 1). Quartz persists until approximately 900 °C and 1.2 GPa for EAT and DAT and approximately 975 °C and 1.3 GPa for MAB, after which hornblende is exhausted around 975 °C and 1.3 GPa for EAT and DAT and 1050 °C and 1.4 GPa for MAB. For DAT and EAT, plagioclase is predicted to be present along most of the 750 °C/GPa gradient, and its proportions decrease steadily at high *P–T*

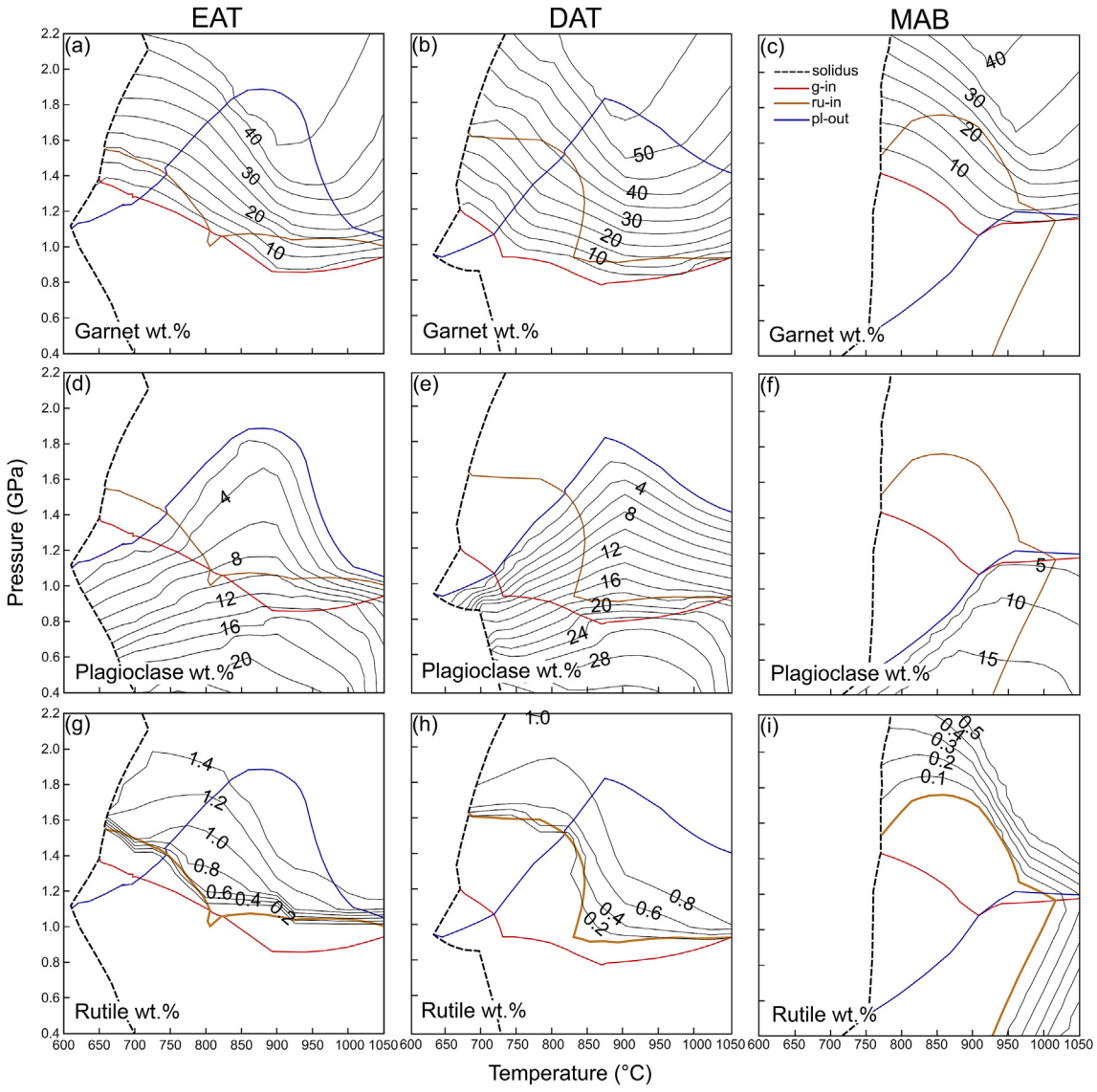


Fig. 3. *P–T* diagrams with contours of weight fractions of garnet, plagioclase, and rutile for the three compositions in Fig. 2. Note that some contours of rutile proportions appear slightly below the rutile-in boundary (g and h); this is an artifact of the lower resolution of the data used for contouring (increments of 25 °C and 0.1 GPa) compared with the higher resolution phase boundaries calculated using Thermocalc (increments of 1–5 °C and 0.01–0.05 GPa). DAT = depleted Archean tholeiite, EAT = enriched Archean tholeiite, MAB = MgO-rich Archean basalt.

where quartz is absent. Beyond hornblende exhaustion, plagioclase continues to be depleted as garnet, clinopyroxene, rutile, and melt proportions increase. The same general trends are predicted for the 1000 °C/GPa gradient in the closed system scenario. Relative to the 750 °C/GPa gradient, quartz is exhausted at slightly lower *P–T* and hornblende persists to higher *P–T*, at least 1000 °C (at 1.0 GPa) for all bulk compositions. Garnet and rutile are stable at relatively higher *P–T* along this gradient, with no garnet predicted for MAB at *P–T* lower than 1050 °C and 1.05 GPa. For all bulk compositions, the 1000 °C/GPa gradient is predicted to produce the highest proportions of plagioclase and melt and the lowest proportions of garnet.

Mineral assemblages and proportions predicted for the open system scenario with melt loss show minor differences relative to the closed system. Residue assemblages (i.e. without melt) for these two scenarios are shown and compared for all *P–T* gradients for DAT as an example (Fig. 4; see also Palin et al., 2016b). Compared to the closed system model for the 500 °C/GPa gradient, the melt loss scenario generally predicts less garnet, clinopyroxene, and rutile, and more plagioclase, hornblende, and quartz. Instead of being exhausted at high temperatures, quartz and plagioclase (not stable for MAB) persist up to at least 1050 °C and 2.1 GPa with relatively minor proportions. Hornblende stability is extended by only 1–2 °C for DAT and EAT, and by 11 °C for MAB. Garnet, clinopyroxene, and rutile decrease to 80–90 wt.% of their closed system weight proportions for DAT and EAT; changes in these minerals are much smaller for MAB. The 750 °C/GPa gradient shows similar changes relative to the closed system scenario, with the major difference for all bulk compositions being the exhaustion of quartz at *P–T* conditions similar to the closed system models and the extension of hornblende stability to at least 1050 °C and 1.4 GPa. Following this trend, greater proportions of hornblende are predicted to remain stable for the 1000 °C/GPa gradient for all bulk compositions. DAT and MAB are predicted to have a similar amount of plagioclase when compared to the closed system scenario, whereas plagioclase proportions are increased for EAT. Unlike the closed system models, no rutile is predicted to be stable along the 1000 °C/GPa gradient for all bulk compositions.

In general, relative to the closed system scenario, the garnet fractionation model predicts that the proportions of all other minerals in the residue increase (as a consequence of renormalizing the proportions of

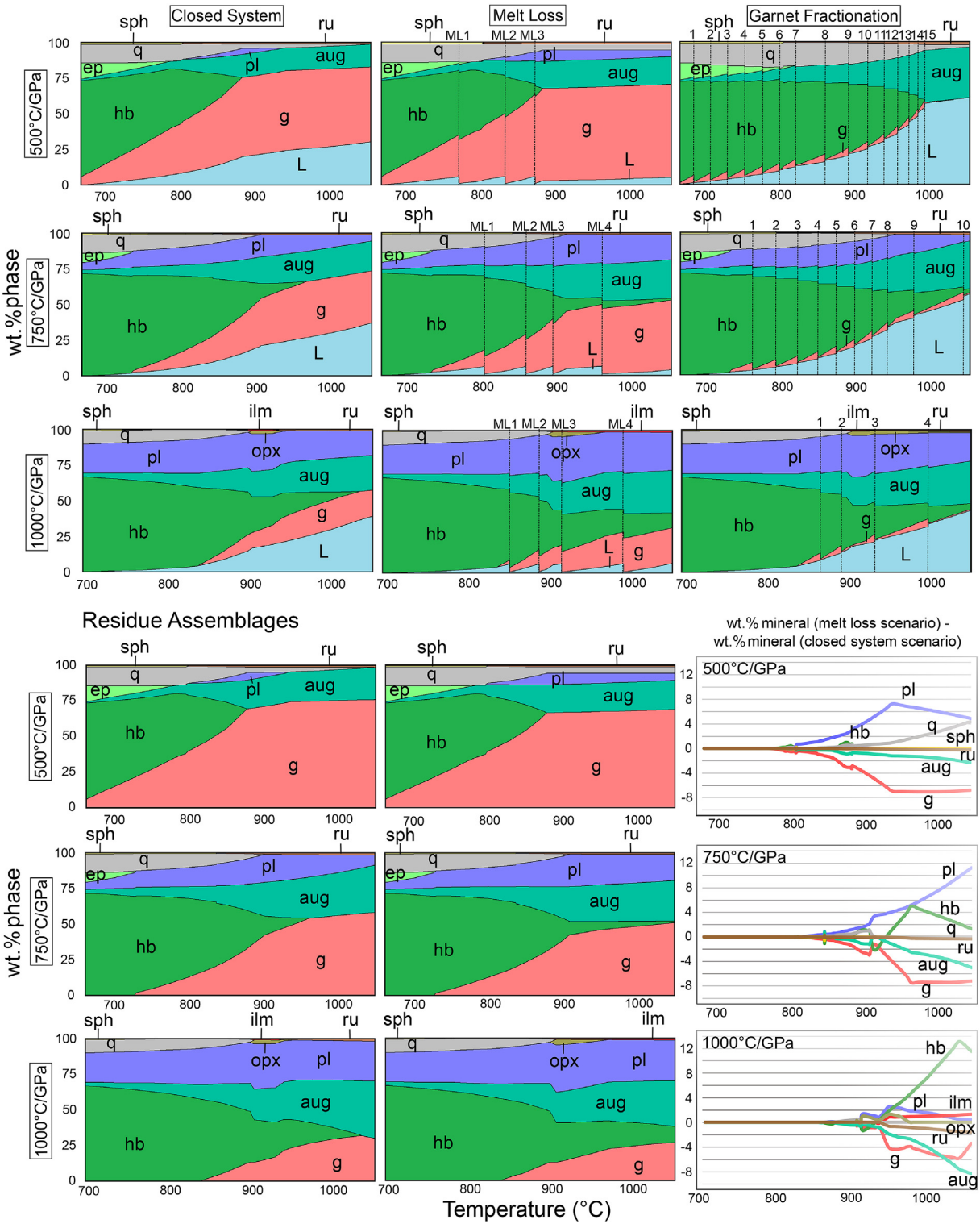


Fig. 4. Temperature–proportion diagrams illustrating the changes in phase weight proportions along the 500 °C/GPa, 750 °C/GPa, and 1000 °C/GPa thermal gradients in the closed system, melt loss, and garnet fractionation scenarios for the DAT (depleted Archean tholeiite) source composition (results for the other source compositions are provided in Supplementary Fig. 1). Additional diagrams are shown excluding melt for the closed system and melt loss scenarios (lower half of figure) along with the relative changes in mineral proportions between the two scenarios (with melt excluded). Phase abbreviations after Holland and Powell (2011). Numbered labels on the melt loss and garnet fractionation diagrams (M1, M2, M3, 1, 2, 3, etc.) designate individual increments of melt or garnet extraction; the vertical dashed lines separate panels of different bulk composition resulting from each extraction.

the phases to a total of 100 wt.% without garnet, as in Fig. 4). Overall, the residue assemblage (minus garnet) shows only minor differences from the closed system scenario, such as the stability of hornblende and quartz extending to higher *P–T*. However, the exception to this is plagioclase, which is not stable along the 500 °C/GPa gradient for all bulk compositions, in contrast to its presence in closed system models for DAT and EAT. With the removal of garnet, the residuum is predicted to be dominated by hornblende until 940–960 °C and 1.88–1.92 GPa, where clinopyroxene becomes most abundant. Along the 750 °C/GPa gradient, plagioclase is stable for DAT and EAT, and it reaches higher proportions in the residue than in the closed system scenario; however, the melt loss model generally predicts the greatest proportions of plagioclase. Consequently, hornblende and clinopyroxene proportions are lower, though they remain the dominant minerals in the residue. Finally, the plagioclase content of the residue is predicted to be highest along the 1000 °C/GPa gradient compared to all other scenarios for DAT and EAT, reaching proportions similar to those of hornblende and clinopyroxene at approximately 900 °C and 0.9 GPa. Given that the 1000 °C/GPa gradient for MAB does not intersect the garnet stability field, the garnet fractionation scenario was not computed.

3.3. Major element compositions of modelled melts

The major element compositions of the modelled melts were evaluated using their CIPW normative ratios of anorthite, albite, and orthoclase (Figs. 5 and 6) to classify them as tonalite, granodiorite, trondhjemite, or granite (O'Connor, 1965; Barker, 1979) and compare them to natural TTG compositions (from Moyen, 2011; the filtered and updated version of this database from Johnson et al., 2019, is used here). For comparison, see also Palin et al. (2016b), where melts from the EAT and DAT compositions were previously classified using this approach. Here, we produced these diagrams to compare melt compositions from the three bulk compositions in the closed system scenario (Fig. 5) and to illustrate the general effects of melt loss and garnet fractionation on melt composition (Fig. 6; shown for DAT only, results from EAT and MAB are available in Supplementary Fig. 2).

Each bulk composition is predicted to produce different melt compositions that are also controlled by the *P–T* gradients, or effectively the pressure, at which the source melted (Fig. 5). In general, for all bulk compositions, melt compositions tend to plot closer to or further within the trondhjemite field with increasing pressure; melts produced along the 500 °C/GPa gradient generally have the highest normative albite content. The 1000 °C/GPa melts plot closest to the anorthite apex and are mainly classified as tonalite or granodiorite. Nevertheless, melts from all gradients trend toward higher normative anorthite proportions with increasing temperature, particularly between 950 °C and 1050 °C.

Of the three source compositions, melts modelled for DAT plot closest to the normative albite apex, with normative orthoclase content decreasing with increasing temperature for all *P–T* gradients. For DAT, the 500 °C/GPa gradient is predicted to produce mainly trondhjemitic melts, whereas melts from the 750 °C/GPa and 1000 °C/GPa gradients mostly plot as granodiorite and tonalite. EAT is predicted to produce different trends, with melts from all gradients showing increasing normative orthoclase proportions with increasing temperature, until an inflection between 750 °C and 850 °C coinciding with the exhaustion of muscovite or biotite, beyond which orthoclase decreases (see also Palin et al., 2016b; White et al., 2017). Thus, melts produced by EAT at temperatures lower than 850 °C for all *P–T* gradients are classified as granitic. Higher temperature melts from the 500 °C/GPa and 750 °C/GPa gradients are trondhjemitic, and those of the 1000 °C/GPa gradient are classified as granodiorite and tonalite. Relative to DAT and EAT, melts predicted to be produced by MAB generally plot closest to the anorthite apex. Melts generated between 750 °C and 850 °C plot in the high-anorthite portion of the granite field and orthoclase content is predicted to decrease with increasing temperature. From 850 °C to 950 °C, the melts are generally granodioritic, with the 500 °C/GPa melts showing the lowest normative anorthite content and plotting closest to the trondhjemite field. Between 950 °C and 1050 °C, melts produced along the 500 °C/GPa and 1000 °C/GPa gradients trend toward higher normative anorthite proportions; however, the 750 °C/GPa melts show increasing normative albite.

Open system behaviour has a minor effect on melt major element composition compared to differences in source bulk composition (Fig. 6). Relative to the closed system scenario, the melt loss scenario is predicted to produce melts above 850 °C that have a higher normative albite content and lower normative orthoclase content, regardless of *P–T* gradient. For DAT and EAT, this effect is greatest for the 1000 °C/GPa gradient, whereas the 500 °C/GPa and 750 °C/GPa gradients are most affected for MAB. Garnet fractionation has an even smaller effect on the major element composition of the melt. Melts produced in this scenario show lower normative anorthite content and this is most apparent at higher temperatures (>850 °C), particularly for the 500 °C/GPa gradient. The melts generated by DAT are most affected, as EAT and MAB melt compositions show little to no change with garnet fractionation.

Of all modelled bulk compositions, the melts produced by DAT show the best agreement with the range of compositions of natural TTGs. For

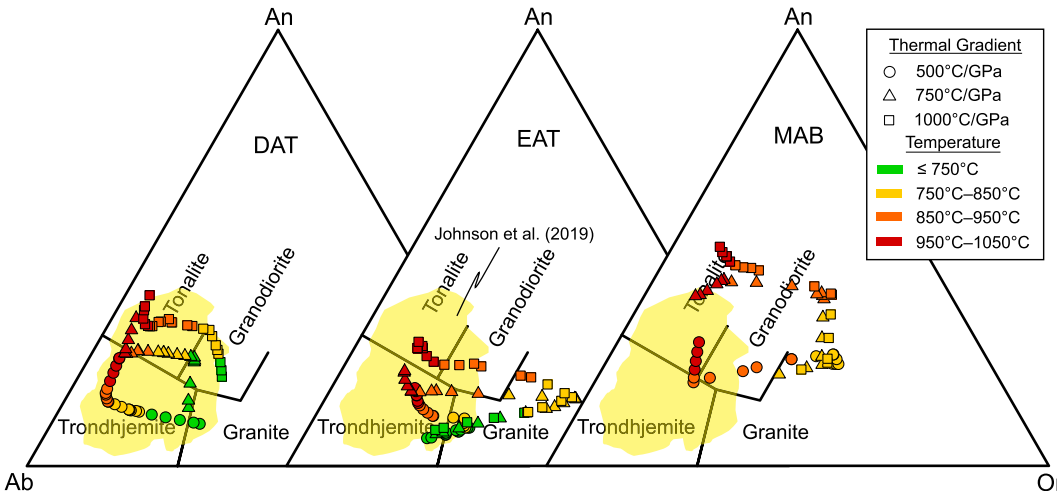


Fig. 5. Granitoid classification diagrams based on normative feldspar content after Barker (1979). Modelled melts from the closed system scenario are plotted for each source composition. Range of natural TTG compositions (after Johnson et al., 2019) is shown in yellow. DAT = depleted Archean tholeiite, EAT = enriched Archean tholeiite, MAB = MgO-rich Archean basalt, An = anorthite, Ab = albite, Or = orthoclase.

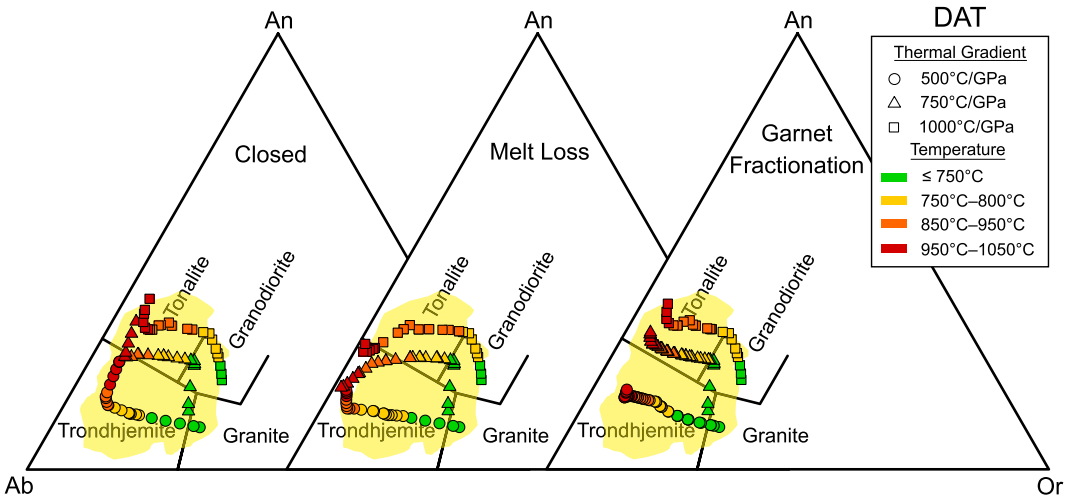


Fig. 6. Granitoid classification diagrams based on normative feldspar content after Barker (1979). Modelled melt compositions are plotted from the closed system, melt loss, and garnet fractionation scenarios for the DAT (depleted Archean tholeiite) bulk composition only. Range of natural TTG compositions (after Johnson et al., 2019) is shown in yellow. An = anorthite, Ab = albite, Or = orthoclase.

EAT and MAB, melts generated at temperatures lower than 850 °C are generally predicted to have more normative orthoclase than the average TTG, and at higher temperatures along the 750 °C/GPa and 1000 °C/GPa gradients, MAB produces melts with higher normative anorthite contents than typical TTGs.

3.4. Trace element compositions of modelled melts

Modelled trends of melt trace elements show some differences among the three bulk compositions (Fig. 7) and can be linked to the modelled behaviour of garnet, plagioclase, and rutile, as discussed above. For the closed system scenario, melt Sr/Y ratios are predicted to reach up to 200 for DAT, 300 for EAT, and 200 for MAB (Fig. 7a–c); the values increase with pressure. Maximum values are near the solidus at ~750 °C for EAT, around 850 °C for DAT, and near 900 °C for MAB. The Sr/Y contours in *P–T* space are curved and mostly concave-up, broadly reflecting the shape of the contours of garnet modal proportions (Fig. 3); however, the curvature is inverted within the plagioclase stability field for DAT and EAT. Within the garnet stability field, MAB Sr/Y contours are predicted to closely match garnet contours, and in the plagioclase-present and garnet-free portion of the diagram, Sr/Y mirrors plagioclase contours. Modelled melt ratios of chondrite-normalized La/Yb have a range up to 320 for EAT, 70 for DAT, and 80 for MAB (Fig. 7d–f), and these elevated values are predicted at the same *P–T* conditions as Sr/Y maxima. The shape of La_N/Yb_N contours is similar to that of garnet contours, and unlike Sr/Y, does not show a change in curvature in the plagioclase stability field. The highest modelled values of Nb in the melt for EAT and DAT, at 44 ppm and 24 ppm respectively, are predicted between 650 °C and 800 °C and 1.2 GPa and 1.5 GPa (Fig. 7g and h). The maximum Nb concentration of 3.4 ppm for MAB is between 800 °C and 900 °C and 1.5 GPa and 1.8 GPa (Fig. 7i). Contours of the concentration of Nb in melt closely follow and are tightly spaced around the rutile-in boundary at lower temperatures (up to 850 °C for EAT and DAT and 950 °C for MAB) and have a similar overall shape to rutile modal proportion contours. The concentration of Nb is predicted to decrease with increasing temperature and pressure, with contours more strongly controlled by temperature.

The effect of bulk composition, *P–T* gradient, and closed vs. open system behaviour are shown for each of the modelled trace elements: Sr, Y, La, Yb, Nb, and Ta (Figs. 8–10). The tabulated results are presented in Supplementary Table 2. Sr/Y is plotted against Y and in general, Sr/Y increases and Y decreases with increasing pressure, with the 500 °C/GPa gradient melts showing the highest Sr/Y (Fig. 8). For DAT and EAT, the melt loss scenario is predicted to produce melts with the lowest maximum Sr/Y (Fig. 8d and e); however, the differences between the melt loss and closed system scenarios (Fig. 8a and b) are minor compared to the garnet fractionation scenario, where maximum Sr/Y may be an order of magnitude higher (Fig. 8g and h). For MAB, the closed system scenario melts are predicted to have lower Sr/Y (Fig. 8c) compared to the melt loss scenario (Fig. 8f) and Sr/Y is highest for the garnet fractionation scenario (Fig. 8i), though the effect is not as extreme compared to the other bulk compositions. In the closed and open system scenarios (Fig. 8a–f), MAB produces the highest Sr/Y melts of all bulk compositions, and the Sr/Y for DAT is slightly higher than EAT. Although melts with the maximum values are predicted to be produced along the 500 °C/GPa gradient, they do not correspond to the maximum pressure of 2.1 GPa explored in the model. In the closed system scenario, maximum Sr/Y is predicted at 1.87 GPa at 936 °C for DAT, 1.93 GPa at 965 °C for EAT, and 1.87 GPa at 934 °C for MAB (Fig. 8a–c; Supplementary Table 2). In the melt loss scenario, the lower maximum Sr/Y for DAT and EAT is produced at only 1.58 GPa at 789 °C and 1.48 GPa at 742 °C respectively (Fig. 8d–f; Supplementary Table 2). In the garnet fractionation scenario, maximum Sr/Y corresponds to melt produced at 1.98 GPa at 991 °C for DAT, 1.95 GPa at 974 °C for EAT, and 1.92 GPa at 960 °C for MAB (Fig. 8g–i; Supplementary Table 2). For all bulk compositions and almost all scenarios, the melts from the 750 °C/GPa and 1000 °C/GPa gradients with the highest Sr/Y are predicted to be produced at or near the peak conditions of 1.4 GPa and 1050 °C and 1.05 GPa and 1050 °C respectively. A notable exception is the 1000 °C/GPa gradient in the closed and melt loss scenarios for MAB (Fig. 8c, f), which shows the opposite trend of Sr/Y decreasing steadily with increasing *P–T* conditions (Supplementary Table 2); the 1000 °C/GPa gradient for MAB also has no stable garnet. Although Sr/Y mainly varies with pressure, some temperature dependence is also evident from the results at 1.4 GPa from each of the 500 °C/GPa and 750 °C/GPa gradients for DAT and EAT, which correspond to 700 °C and 1050 °C respectively. For the closed system and melt loss scenarios, the value of Sr/Y at 1050 °C is predicted to be up to two times greater than that at 700 °C; however, in the garnet fractionation scenario, Sr/Y is one order of magnitude greater at 1050 °C. At ~1.4 GPa along the 500 °C/GPa and 750 °C/GPa gradients for MAB, Sr/Y at 1050 °C is less than double the value at 700 °C for all modelled scenarios.

Chondrite normalized La/Yb vs. Yb of the modelled melts (Fig. 9) follow trends similar to Sr/Y vs. Y, with maximum values predicted to correspond to melts produced along the 500 °C/GPa gradient in all scenarios. The closed (Fig. 9a–c) and melt loss (Fig. 9d–f) scenarios yield similar results for all bulk compositions, whereas garnet fractionation (Fig. 9g–i) is predicted to produce La_N/Yb_N two to three orders of

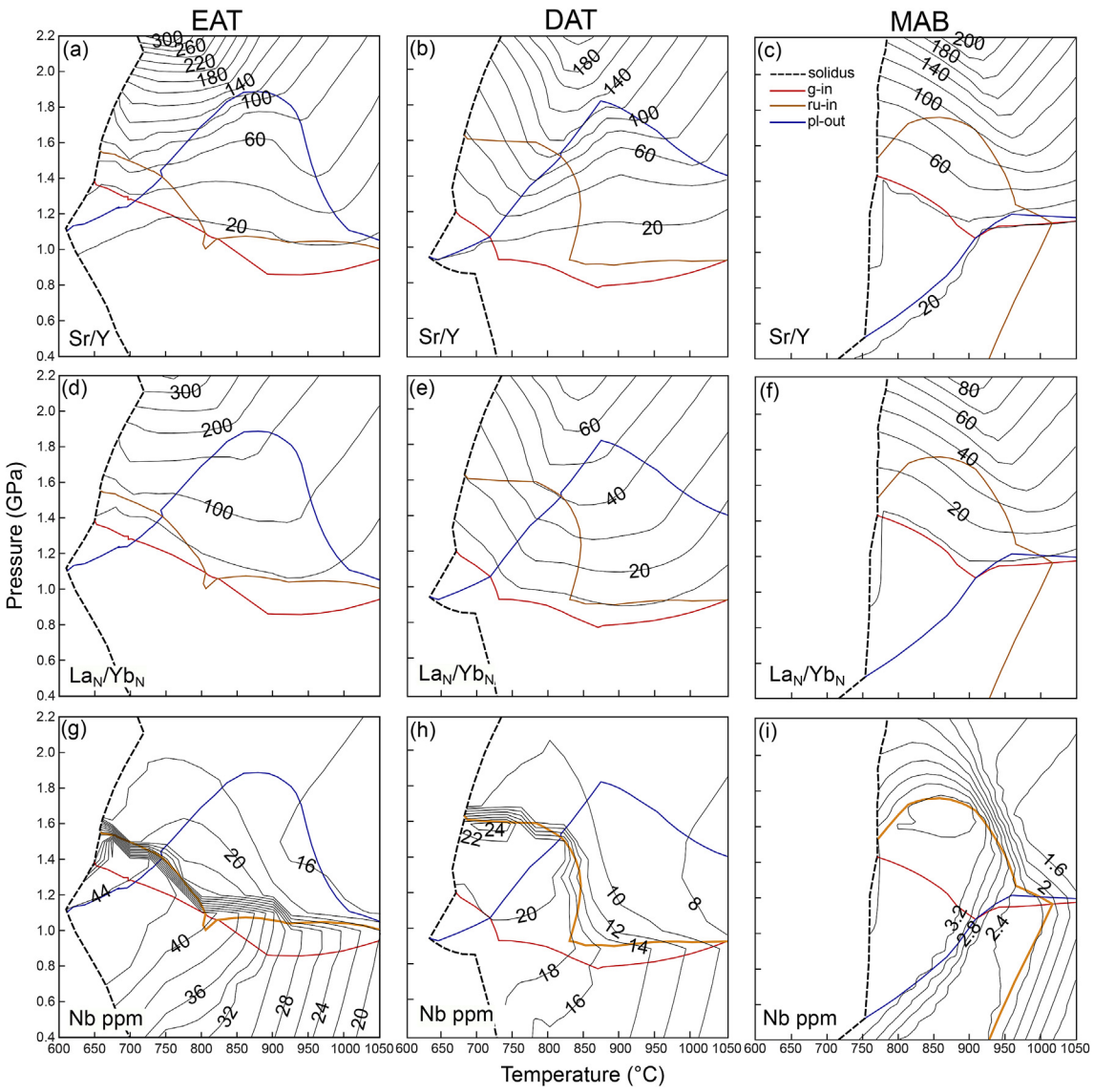


Fig. 7. *P–T* diagrams with contours of Sr/Y, La_N/Yb_N, and concentration of Nb (ppm) in the melt. DAT = depleted Archean tholeiite, EAT = enriched Archean tholeiite, MAB = MgO-rich Archean basalt.

magnitude greater in comparison. In contrast to Sr/Y, melts derived from EAT have the highest La_N/Yb_N values in all scenarios (Fig. 9b, e, h); however, like Sr/Y, maximum La_N/Yb_N does not correspond to peak *P–T*. Melts produced by DAT and EAT along the 500 °C/GPa gradient reach maximum La_N/Yb_N at approximately 1.75 GPa and 877 °C for both the closed and open systems (Fig. 9a, b, d, e; Supplementary Table 2), which makes La_N/Yb_N decoupled from Sr/Y. However, for this *P–T* gradient, Sr/Y and La_N/Yb_N are coupled in the garnet fractionation scenario (Fig. 9g and h). In general, the 750 °C/GPa and 1000 °C/GPa gradient melts for DAT and EAT are predicted to reach maximum La_N/Yb_N at slightly lower *P–T* than maximum Sr/Y, typically by ≤ 0.1 GPa and ≤75 °C or 100 °C, depending on the gradient. For all *P–T* gradients and modelled scenarios, the La_N/Yb_N of melts produced by MAB are coupled to Sr/Y (Fig. 9c, f, i). Comparing La_N/Yb_N predicted at different temperatures but similar pressures from the 500 °C/GPa and 750 °C/GPa gradients yields similar results to Sr/Y. For DAT and EAT, La_N/Yb_N at 1.4 GPa and 1050 °C is up to three times greater than that at 1.4 GPa and 700 °C, and in the garnet fractionation scenario, the difference becomes two orders of magnitude. The temperature dependence is not as great for MAB, with La_N/Yb_N up to four times greater at high temperature compared to low temperature.

The Nb concentrations of the melts are plotted against Ta concentrations and, for each *P–T* gradient, the lowest Nb and Ta correspond to maximum *P–T* in all cases (Fig. 10). Differences between the closed system, melt loss, and garnet fractionation scenarios are minor for all bulk compositions, and melts produced by EAT are predicted to have the highest and largest range of Nb and Ta concentrations (Fig. 10b, e, h); melts produced from MAB have the lowest and smallest range of concentrations (Fig. 10c, f, i). For DAT and EAT, Ta concentrations are overall higher with increasing thermal gradient and the opposite is predicted for MAB. The range of concentrations of Nb in the melt is similar for each gradient; however, in the melt loss scenario for all bulk compositions (Fig. 10d–f) and the garnet fractionation scenario for EAT (Figs. 10h), 1000 °C/GPa gradient melts are restricted to higher Nb. Almost all *P–T* gradients for each of the bulk compositions show an initial increase in Nb and Ta with increasing *P–T*, with maximum Nb typically produced at lower *P–T* than maximum Ta. With further *P–T* increase, both Nb and Ta decrease, and the concentrations predicted for different *P–T* gradients, particularly 500 °C/GPa and 750 °C/GPa, converge toward similar values.

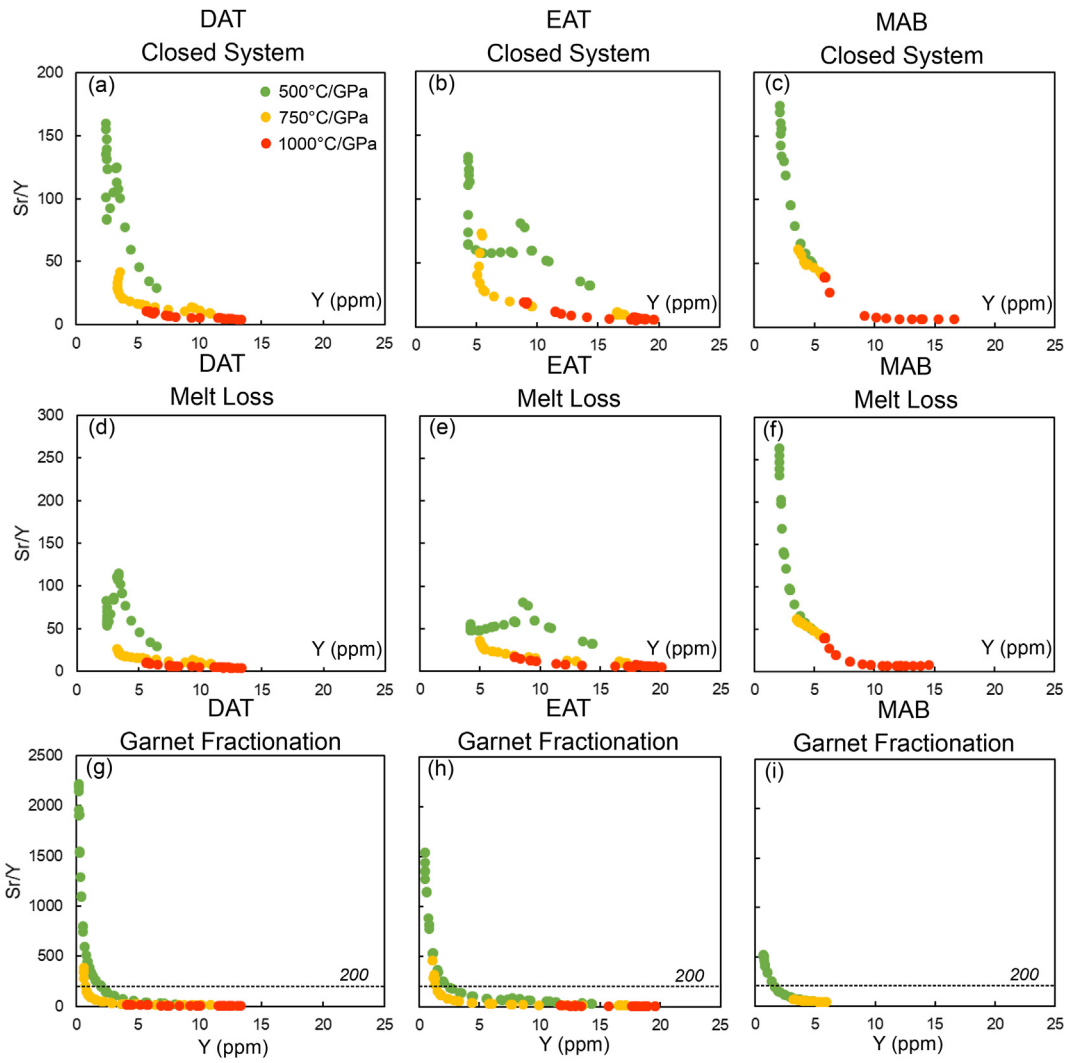


Fig. 8. Plots of Sr/Y vs. Y of modelled melts from each of the three compositions for each of the three scenarios. The garnet fractionation scenario was not modelled for the 1000 °C/GPa gradient for MAB due to lack of garnet. DAT = depleted Archean tholeiite, EAT = enriched Archean tholeiite, MAB = MgO-rich Archean basalt.

4. Discussion

4.1. Limitations of the models

The modelled melt compositions presented here are subject to the limitations inherent to phase equilibrium modelling (e.g. Powell and Holland, 2008; Palin et al., 2016b; Forshaw et al., 2019; Lanari and Duesterhoeft, 2019), including the assumption of equilibrium (major and trace components) among all phases during melting. Although the clinopyroxene model we use is considered appropriate across most of the investigated *P*–*T* conditions, it generally underestimates Na substitution at high pressure–low temperature conditions, which causes a shift in topology in this region of the phase diagram (Green et al., 2016). In addition, the *a*–*x* models used in our models do not consider Ti substitution in clinopyroxene or Ti incorporation in the melt (e.g. Ryerson and Watson, 1987; Forshaw et al., 2019). This results in an overestimation of the proportion of rutile in our models relative to nature, which in turn would cause concentrations of Nb and Ta in the melt to be lower in the models. For example, rutile is predicted to be stable to 0.4 GPa at high temperatures in the model for MAB (Fig. 3i), which may not be realistic. Given that the Fe^{2+}/Fe^{3+} ratio of MAB is unknown, this introduces further uncertainty to the *P*–*T* extent of the rutile stability field and modal proportions of rutile, which in turn adds uncertainty to the modelled concentrations of Nb and Ta in the melt. The Fe^{2+}/Fe^{3+} ratio may also have minor effects on the stability fields of the other minerals included in the modelling, as has been demonstrated for pelitic bulk compositions (Boger et al., 2012).

The partition coefficients used in the models (from Bédard, 2006) to calculate the concentrations of trace elements in the modelled melts are subject to uncertainty and are not constant values in nature. Although the values used are considered to be suitable for partial melting of metabasites (Bédard, 2006), partition coefficients generally vary with changes in temperature, pressure, melt composition, and mineral composition (Blundy and Wood, 2003). Nevertheless, we expect that the modelled trends in the trace element compositions of the melts are robust, as they are driven by strongly compatible behaviour between certain elements and minerals, and this behaviour should not change significantly with varying partition coefficients. For instance, an experimental study (Nicholls and Harris, 1980) of REE partitioning between andesitic melts and garnet at different temperatures reported a range in partition coefficients from ~10 to ~45 for Yb, which encompasses the value of 23.2 used in our models. Despite this range, all values are an order of magnitude greater than 1, indicating that Yb would be readily incorporated into garnet regardless of temperature. Consequently, uncertainty and variability in partition coefficients would affect the calculated concentrations of trace elements in the modelled melts, but the overall effect of melting in the garnet, plagioclase, or rutile stability field and the trends in the trace element concentrations in melt would be the same.

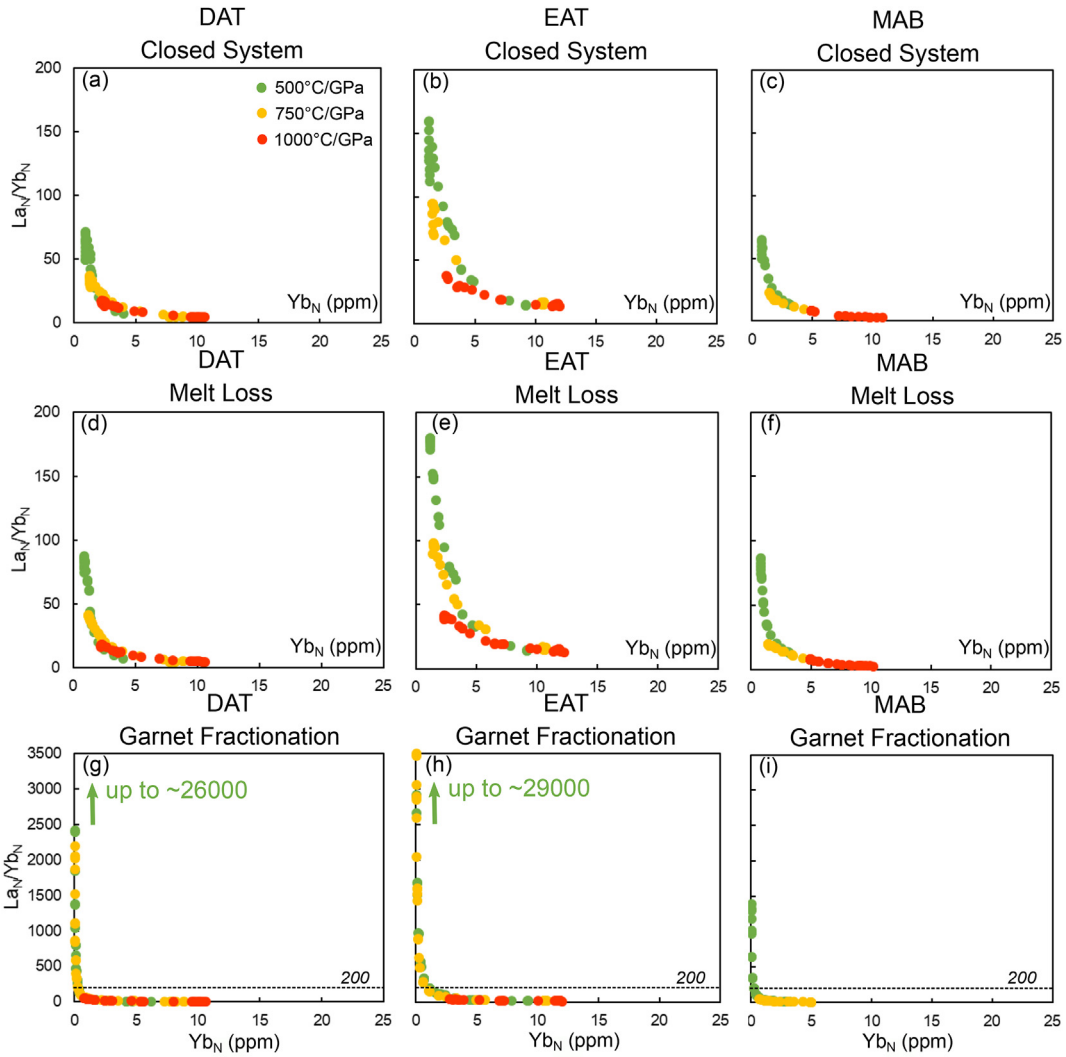


Fig. 9. Plots of La_N/Yb_N vs. Yb_N of modelled melts from each of the three compositions for each of the three scenarios. The garnet fractionation scenario was not modelled for the 1000 °C/GPa gradient for MAB due to lack of garnet. DAT = depleted Archean tholeiite, EAT = enriched Archean tholeiite, MAB = MgO-rich Archean basalt.

Finally, measured concentrations of the HREE in hornblende in intermediate to metabasic migmatites are quite high relative to values predicted using existing partition coefficients (e.g. Reichardt and Weinberg, 2012; Yakymchuk et al., 2019), which suggests that hornblende may be a more important sink for the HREE in the residue in nature relative to the models.

Further limitations arise from assumptions made to simplify the natural process of partial melting of metamorphic rocks. In our models, we do not consider the effect of accessory minerals, which are commonly apatite and zircon in metabasites, on melt trace element compositions. Zircon is unlikely to have a significant effect because the concentration of Zr in Archean basalts is commonly relatively low (≤100 ppm; Condie, 1985) resulting in little to no zircon in the source of TTGs. Relatively higher concentrations of P in Archean basalts (Condie, 1985) may stabilize apatite, which may be a significant reservoir for Y and REEs due to the high partition coefficients for these elements between apatite and melt (Bédard, 2006). However, apatite solubility is expected to be small for metaluminous melt compositions (e.g. Watson and Capobianco, 1981; Pichavant et al., 1992). Therefore, residual apatite is expected to slightly increase the Sr/Y composition of the melt relative to the scenarios modelled here, but it is not expected to significantly affect the La/Yb ratio considering the similar partition coefficients for the REE between melt and apatite (Bédard, 2006). In addition, some proportion of apatite and zircon may be trapped within peritectic phases such as garnet and not accessible to the melt (Watson et al., 1989; Sawyer, 1999), making the role of accessory minerals as trace element reservoirs difficult to model for a general scenario. Sequestration of rutile in unreactive or growing minerals could cause sequestration of Nb and Ta and consequently lower concentrations of these elements in the melt. Given that rutile preferentially incorporates Ta over Nb, this would cause the bulk and melt Nb/Ta to shift toward higher values.

In the garnet fractionation models, we assume complete sequestration of garnet cores, although realistically, limited thermally-activated diffusive exchange between garnet and other phases would be possible. Major elements such as Fe, Mg, and to a lesser extent, Ca, would be expected to diffuse readily, given their mobility in garnet at high temperatures (Carlson, 2006). In the models, the bulk compositions typically become progressively depleted in these elements as garnet is removed from the effective bulk composition (Lanari and Engi, 2017) with increasing temperature, particularly along the 500 °C/GPa gradient, which is predicted to produce the most garnet. This affects the *P–T* stability fields of other minerals that require these elements. For example, the 500 °C/GPa gradient for DAT and EAT intersects the plagioclase stability field in the closed and melt loss scenarios, but not in the garnet fractionation model. Therefore, in the garnet fractionation scenario, the plagioclase content of the residue may be underestimated and the Sr concentration of the melt

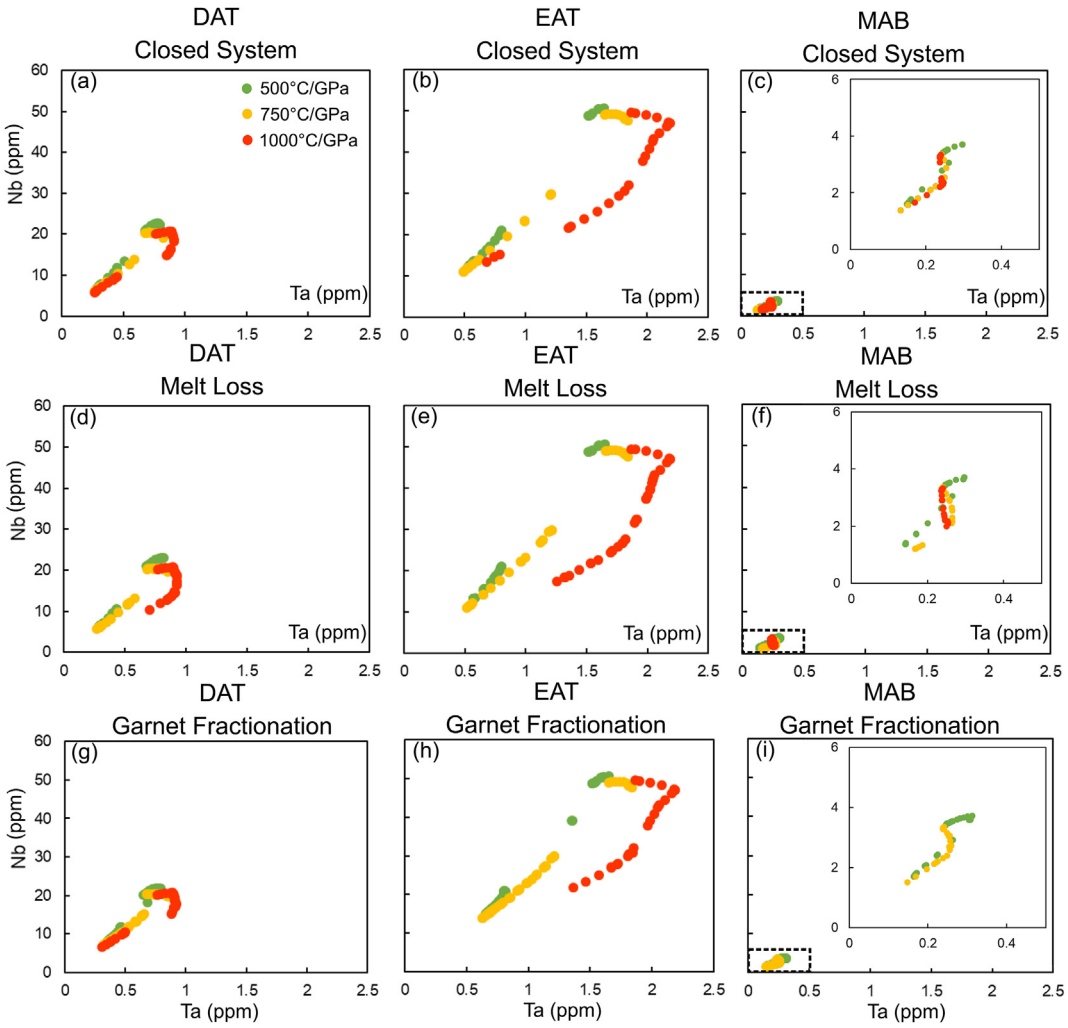


Fig. 10. Plots of Nb vs. Ta of modelled melts from each of the three compositions for each of the three scenarios. The garnet fractionation scenario was not modelled for the 1000 °C/GPa gradient for MAB due to lack of garnet. DAT = depleted Archean tholeiite, EAT = enriched Archean tholeiite, MAB = MgO-rich Archean basalt.

may be overestimated. In addition, although trivalent cations (Y, HREE) in garnet diffuse about an order of magnitude slower than divalent cations (Carlson, 2012), these elements may not remain completely sequestered in the cores depending on the temperature, duration of heating, and size of the garnet. This would cause melt concentrations of the trace elements enriched in garnet, Y and Yb, to be higher and Sr/Y and La_N/Yb_N ratios of melt to be lower. This may be particularly important in Archean cratons that remained at high temperatures for long durations (e.g. Kelly and Harley, 2005; Moser et al., 2008; Gardiner et al., 2019). Thus, our garnet fractionation model is likely an end-member representation of the natural process.

An important difference between the modelled melts and natural TTGs is that the models produce melt compositions in equilibrium with the residue in the source metamorphic rock, with no consideration of the processes that would modify the composition of the melt during extraction from the source, magma ascent, and emplacement. One potentially important process is the entrainment and subsequent dissolution of peritectic minerals in the melt during ascent. Evidence for peritectic garnet entrainment has been identified in natural felsic igneous rocks (Stevens et al., 2007; Taylor and Stevens, 2010), and the result of this would be a new melt composition that falls on a mixing line between the garnet and initial melt compositions (Moyen et al., 2009). This process could have a significant effect on the concentrations of trace elements in the melt, as dissolution of garnet would add Y and Yb, thereby lowering the Sr/Y and La_N/Yb_N ratios. Furthermore, any rutile inclusions within the entrained garnet could also break down, contributing Nb and Ta to the melt. Another potentially important process is mixing of the melts with other contemporaneous melts from different sources, such as the mantle or possibly heterogenous lower crust. The effect of magma mixing on trace element concentrations would vary depending on the source and degree of fractionation of the contaminating magma. Fractional crystallisation of minerals out of migrating melt that feeds TTG plutons has the potential to affect trace element content; however, the effect may be small. The relative timing of crystal fractionation of different minerals is crucial, and investigations of tonalite melting by thermodynamic modelling (Holland et al., 2018) and experiments (Stern et al., 1975; Schmidt and Thompson, 1996) have shown that plagioclase, hornblende, and possibly clinopyroxene are likely to be the most significant early (T > 900 °C) fractionating phases at pressures below 1.0 GPa. At higher pressures, melting experiments (Schmidt and Thompson, 1996) show that epidote and garnet may become more important, with garnet stable at a minimum pressure of approximately 1.4 GPa. Fractionation of plagioclase would cause a depletion of Sr, fractionation of epidote would remove Sr, Y and REEs (preferentially LREEs), and fractionation of garnet would reduce the concentrations of Y and HREE in the melt. However, fractionation modelling of tonalitic melts (Moyen et al., 2009) has indicated that changes to Sr and Y due to hornblende, epidote, and garnet fractionation would be minor, as the relatively low concentrations of FeO

and MgO in the melt would inhibit significant production of these minerals. Furthermore, geochemical trends in suites of granitoid rocks commonly cannot be attributed to fractionation alone (Clemens et al., 2009), and separation of relatively low-density silicate minerals from high-viscosity, silica-rich melts may be difficult (Glazner, 2014; Clemens, 2015).

4.2. Comparison of modelled melts to natural TTGs

In some scenarios modelled here, the trace element compositions of the melts match the range of the compositional groups of natural TTGs as defined by Moyen (2011) and the compilation of TTG geochemical data of Johnson et al. (2019), although there are some inconsistencies (Fig. 11). The Sr/Y and La_N/Yb_N ratios of melts from the closed-system models are shown in comparison to the high pressure, medium pressure, and low pressure TTG groups as defined by Moyen (2011) (Fig. 11). The compositional differences that define the groups are considered to signify the different depths, or pressures, of melting, with low pressure representing 1.0–1.2 GPa, medium pressure representing approximately 1.5 GPa, and high pressure representing ≥2.0 GPa (Moyen, 2011). Notably, the pressures that Moyen (2011) assigned to these groups are based on the stabilities of plagioclase, garnet, and rutile observed during melting experiments of basalts (Moyen and Stevens, 2006); calculating the stability fields of these minerals by phase equilibrium modelling has produced different results (e.g. Palin et al., 2016a,b; Johnson et al., 2017). The groups are generally distinguished by Sr/Y and La_N/Yb_N, which are inferred to be higher for TTGs generated at higher pressures (Moyen, 2011). Overall, this trend is replicated in the models (Figs. 8 and 9), with Sr/Y and La_N/Yb_N of the melts increasing with increasing *P–T* and reaching the highest values along the 500 °C/GPa gradient, which corresponds to the highest pressures. Most of the results from the 1000 °C/GPa gradient have lower Sr/Y and La_N/Yb_N than the low pressure TTG group, with a few exceptions from EAT and MAB. Melts modelled along the 750 °C/GPa gradient plot within both the low pressure and medium pressure composition ranges, with those within the latter group generally corresponding to higher pressures. Finally, the 500 °C/GPa modelled melt compositions are most consistent with the medium pressure group, with the highest Sr/Y and La_N/Yb_N melts for all bulk compositions reaching values in the overlap between medium pressure and high pressure TTGs. Notably, melts with the maximum Sr/Y and La_N/Yb_N are not produced at the maximum pressure considered in the model, which reflects the influence of temperature on garnet and plagioclase modal proportions (Figs. 3 and 7). The compositions of melts produced in the melt loss model are similar to the compositions measured of the different TTG groups, though with slightly lower Sr/Y and slightly higher La_N/Yb_N (Fig. 8d–f and 9d–f). However, in the garnet fractionation model, some melts produced at elevated *P–T* conditions have Sr/Y and La_N/Yb_N higher than all natural TTGs. The TTG groups of Moyen (2011) were not designed to encompass the compositions of all natural TTGs, and therefore the maximum Sr/Y of approximately 300 and La_N/Yb_N of

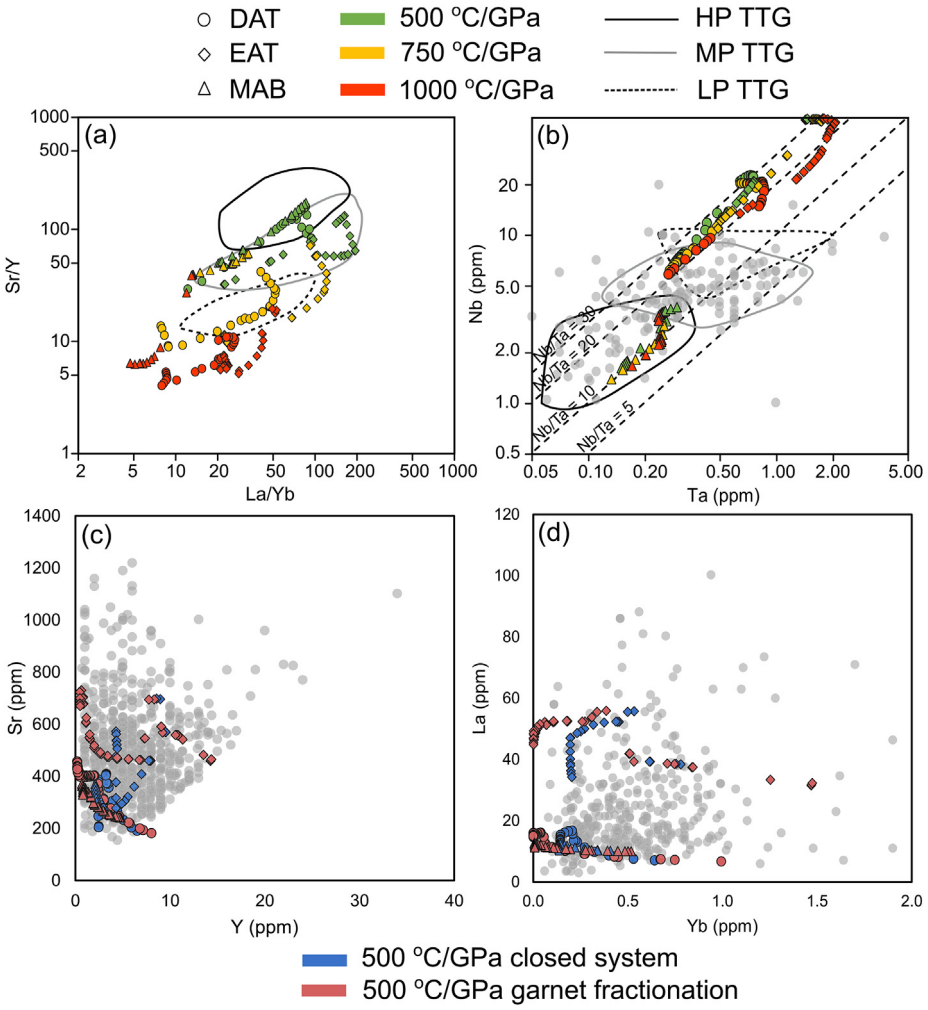


Fig. 11. Trace element compositions of modelled melts compared to (a and b) the high pressure (HP), medium pressure (MP), and low pressure (LP) TTG groups (Moyen, 2011) and (b–d) natural TTG data (grey symbols, after Johnson et al., 2019). Diagrams in (a) and (b) include data from the closed system scenario only. DAT = depleted Archean tholeiite, EAT = enriched Archean tholeiite, MAB = MgO-rich Archean basalt.

approximately 200 for the high pressure group are exceeded by a small percentage of the TTGs in the Johnson et al. (2019) compilation. Although the maximum modelled Sr/Y of melts from DAT and EAT of ~2200 and ~1500 respectively, produced along the 500 °C/GPa gradient, are higher than the highest Sr/Y of the natural samples at 1166, the order of magnitude is consistent (Fig. 8g and h). However, the maximum La_N/Yb_N of the modelled melt is one (MAB) to two (DAT and EAT) orders of magnitude greater (Fig. 9g–i) than the highest La_N/Yb_N in the compilation of Johnson et al. (2019) of 527. Similarly, modelled melts from DAT and EAT in the garnet fractionation scenario along the high *P–T* portion of the 750 °C/GPa gradient have maximum Sr/Y consistent with the high pressure group of TTGs (Fig. 8g and h), and maximum La_N/Yb_N an order of magnitude greater than natural TTGs (Fig. 9g and h). Thus, our garnet fractionation model may somewhat overestimate Sr/Y and greatly overestimate La_N/Yb_N relative to nature. The reason is apparent in the concentrations of these elements in modelled melts from the 500 °C/GPa gradient, which are generally in agreement with data from TTGs, except for the very low Y and Yb predicted in the garnet fractionation scenario (Fig. 11c and d). This suggests that diffusion of these elements out of the garnet cores and entrainment of peritectic garnet within natural melts may be common processes, resulting in increased concentrations of Y and Yb in natural melts relative to our models.

The Nb and Ta systematics of the modelled melts from the closed system scenario are shown in comparison to the TTG groups and natural data (Fig. 11b). The groups are relatively well-defined by their Nb and Ta concentrations, which decrease with increasing pressure (Moyen, 2011). Although the Nb/Ta ratio of the modelled melts is consistent with observations from TTGs, their Nb and Ta concentrations do not show the same trend with increasing pressure as the TTG groups. All modelled melts from the three *P–T* gradients for MAB plot within the high pressure group, despite being produced at a range of pressures from 0.75 GPa to 2.1 GPa. In contrast, all of the concentrations of Nb and Ta in modelled melts from EAT are higher than any of the TTG groups, whereas melts from DAT overlap with the medium and low pressure groups. For each bulk composition, the different *P–T* gradients do not produce significantly different results. Given that each gradient corresponds to a different range of pressures, this indicates that pressure is not the main control on concentrations of Nb and Ta in the modelled melts. This is consistent with the stability of rutile in the models: although rutile becomes stable at high pressures, its modal proportions (Fig. 3) are controlled by the temperature-dependent breakdown of hornblende, the only other stable Ti-bearing phase in the rutile stability field. Therefore, changes in source bulk composition contribute to the greatest variety in Nb and Ta in the models. However, when compared to the natural TTG data, most modelled melts from EAT and some from DAT have Nb and Ta concentrations that exceed the observed range. Given that rutile proportions are likely overestimated in the models (see section 4.1), which should result in an underestimation of Nb and Ta in the melt, this result may be indicative of the importance of rutile sequestration in natural systems. However, a more likely explanation is that the Nb and Ta concentrations assigned to EAT and DAT due to unavailable data (see section 2.1) are not representative of the average depleted or enriched Archean tholeiite; high-Nb basalts (such as the Coucal basalts, considered here to be analogous to EAT) may have been scarce. Although the concentrations of Nb and Ta in the modelled melts may not be realistic, the trends outlined above are independent of this and are therefore more meaningful.

4.3. Implications for interpreting TTG trace element systematics

4.3.1. The role of bulk composition

The mafic bulk compositions modelled here as TTG sources yield melts of different major and trace element compositions. In terms of major elements (Fig. 5), DAT produces melts with normative feldspar compositions most comparable with natural TTGs, whereas the modelled melts of EAT are comparable only at high temperatures. Melts produced by MAB have the poorest match with natural TTGs. The EAT and MAB compositions produce some melts with higher normative orthoclase content than typical TTGs, which may result from the higher K_2O/N_2O of these sources compared to DAT (Table 1). However, these melts are generally produced by a low degree of partial melting at low temperature. At proportions less than 7 mol% in a static system (Rosenberg and Handy, 2005), and potentially lower in a system undergoing syn-anatectic deformation (Brown, 2013), melt may not form a connected network along grain boundaries to allow extraction from the source. For each of the thermal gradients, 500 °C/GPa, 750 °C/GPa, and 1000 °C/GPa, melt reaches 7 mol% at ~750 °C, ~820 °C, and ~830 °C for EAT and ~880 °C, ~900 °C, and ~880 °C for MAB. Therefore, some of the melts with high normative orthoclase would not be expected to be preserved in the geological record. Most of the melts produced by MAB at high temperatures along the 750 °C/GPa and 1000 °C/GPa gradients have a higher normative anorthite content than natural TTGs. Given that MAB has a similar wt.% CaO to DAT and EAT (Fig. 1), these melt compositions may reflect the relatively low Na_2O concentration of MAB (Table 1). Overall, the different mafic source compositions produce a range of melt compositions in terms of normative albite, anorthite, and orthoclase (Fig. 5), which may be controlled by the K_2O and Na_2O concentrations of the sources.

The trace element compositions of the melts are predicted by the models to be affected both by differences in the concentration of trace elements in the source and the residue mineral assemblage. The high concentration of La in EAT allows the melts to reach higher La_N/Yb_N and higher concentrations of La in melt than the other bulk compositions (Fig. 11d), suggesting that a LREE-enriched source is likely necessary to produce the most LREE-enriched natural TTGs (cf. Moyen and Martin, 2012); the same may also be true for Sr and Y (Fig. 11c). However, despite their relative depletion in La, Yb, Sr, and Y, DAT and MAB generate melts with concentrations of these elements comparable to TTGs (Fig. 11c and d). The Nb and Ta systematics of modelled melts are strongly controlled by the concentrations of Nb and Ta in the source, though this effect may be exaggerated by the large range of source Nb and Ta selected for this study. The reduced garnet stability field in the MAB composition relative to DAT and EAT in the *P–T* range of interest has a significant effect on Sr/Y and La_N/Yb_N of the melt in the garnet fractionation scenario. The maximum Sr/Y and La_N/Yb_N of melts produced by MAB, which are associated with the 500 °C/GPa gradient, are an order of magnitude less than those of DAT and EAT. Additionally, with garnet fractionation, melts produced along the 750 °C/GPa gradient by DAT and EAT reach Sr/Y and La_N/Yb_N consistent with the high pressure TTG group of Moyen (2011), whereas those of MAB remain relatively low. Although these values are likely overestimated in our models, this trend indicates that the effect of garnet fractionation is weaker for MAB as a result of lower modal proportions of garnet.

4.3.2. The role of open system processes

Of the open system processes investigated here, melt loss and garnet fractionation, garnet fractionation potentially has the most significant consequences for the trace element composition of TTGs. The relatively small decrease in Sr/Y for DAT and EAT in the melt loss scenario can be attributed mainly to lower Sr concentrations due to the increased stability of plagioclase to higher *P–T* (Fig. 4). In contrast, the increased Sr/Y for melts produced by MAB and La_N/Yb_N of the modelled melts for all bulk compositions is the result of increased Sr and La melt concentrations likely caused by the smaller proportions of melt present in the system. The relatively minor effect of melt loss can be linked to the moderate partition coefficients between the melt and residue (or bulk distribution coefficient) for the elements of interest compared to the large partition coefficients for Y and Yb for garnet. Removal of garnet from the model has a greater potential to affect the bulk concentration of these trace elements, particularly for *P–T* gradients predicted to have high modal proportions of garnet. Although garnet fractionation, as modelled here, is

an extreme scenario, the trends obtained for Sr/Y and La_N/Yb_N suggest that a more subdued version of this process in nature may be important.

The closed system scenario fails to produce melts with Sr/Y considered to be characteristic of TTGs produced at 2.0 GPa or greater, despite 2.1 GPa being the maximum pressure investigated for the 500 °C/GPa gradient. Furthermore, Sr/Y is predicted in the models to decrease after reaching a peak value at approximately 1.9 GPa, which is linked to the concave-up shape of garnet modal proportion contours in *P–T* space (Fig. 3) — the elevated ratios observed in natural TTGs would not be achieved by melting at higher pressures along this gradient. Therefore, our results suggest that garnet fractionation in the source may be needed to yield melts with Sr/Y ratios significantly greater than 200. In contrast, the La_N/Yb_N ratios of modelled melts from the closed system scenario cover the range of La_N/Yb_N represented by the three TTG groups of Moyen (2011). Owing to their high La concentrations, melts produced by EAT reproduce the high La_N/Yb_N expected of the medium and high pressure groups, whereas those of DAT and MAB do not. However, with garnet fractionation, it is conceivable that less LREE-enriched sources such as DAT and MAB could generate melts with elevated La_N/Yb_N (i.e. greater than 100). Another consequence of garnet fractionation is the potential for more temperature-dependent variation of Sr/Y and La_N/Yb_N ratios compared to the closed system and melt loss scenarios. Given the moderate temperature dependence of garnet production predicted by the models (Fig. 3), garnet growth and Y and Yb fractionation away from the reactive bulk composition may occur by an isobaric temperature increase. The effect of this was described above in the results of the 500 °C/GPa and 750 °C/GPa gradients for DAT and EAT: at the same pressure, garnet fractionation caused Sr/Y and La_N/Yb_N to increase by one to two orders of magnitude from low to high temperature. This allowed Sr/Y and La_N/Yb_N at 1.4 GPa to exceed values expected for melts produced at $\geq$ 2.0 GPa.

4.4. Implications for linking TTG trace elements to depth of melting

Three geodynamic models have been proposed to explain the generation of TTGs in the Archean, and each implies melting of metabasites at different depths. The first scenario is reworking of thickened mafic crust, similar to modern oceanic plateaux, through processes unrelated to modern-style and horizontally-driven plate tectonics, which include mantle overturn, mantle plumes, and delamination of residual lower crust (Bédard, 2006, 2018; Johnson et al., 2014; Sizova et al., 2015). The suggested thickness of Archean oceanic crust ranges from 25 km to 45 km based on the estimated degree of melting of the relatively hot Archean mantle (Herzberg et al., 2010; Herzberg and Rudnick, 2012), indicating a maximum depth of TTG generation of 45 km in this model. A second model invokes thickening of Archean mafic crust, which may be achieved in an arc environment (Nagel et al., 2012) or in a long-lived volcanic system driven by a mantle plume (Bédard et al., 2013). Melting would therefore be possible at depths greater than 45 km – up to 60 km has been proposed (Bédard et al., 2013). The third scenario is melting of subducted mafic crust, a process that is inferred in modern subduction zones from the presence of adakites, which have geochemical characteristics indicative of melting of a garnet-bearing metabasite source (Drummond et al., 1996). Adakites have been proposed to be modern analogues of TTGs based on several geochemical similarities, leading to the interpretation that TTGs were produced by melting of subducted slabs (Drummond and Defant, 1990; Hastie et al., 2010). Given that mantle temperatures are inferred to have been higher in the Archean relative to modern Earth (Abbott et al., 1994; Herzberg et al., 2010), melting of subducting slabs may have been more common in the Archean (Moyen and Stevens, 2006). However, other workers oppose the slab melting model for TTG formation (e.g., Bédard, 2006) based on a lack of geochemical evidence for mantle interaction in many TTGs (Martin et al., 2005) and the potential for dehydration of the subducting slab before reaching solidus temperatures during hot subduction (Harry and Green, 1999). Our models cannot necessarily be used to test these hypotheses, given that we investigated only three Archean basalt compositions that may not fully encompass the source compositions expected for these different geodynamic environments. However, these scenarios are differentiated by the depth of melting, and our results have important implications for using particular geochemical characteristics of TTGs as proxies for pressure at the source.

In general, our modelled melt compositions from the lowest pressure gradient, 1000 °C/GPa, are consistent with geochemical signatures attributed to low pressure melting. These melts are produced in the models at pressures up to 1.0 GPa, which corresponds to a depth of ~34 km assuming overlying material is mafic with a density of 3000 kg/m^3. These melts are predicted to have low Sr/Y and La_N/Yb_N ratios in every scenario, consistent with or lower than the low pressure group of TTGs of Moyen (2011), even for bulk compositions with a small proportion of stable garnet in this pressure range (DAT and EAT). Other basalt bulk compositions not represented here may stabilize garnet at lower pressures than our models; for instance, phase equilibrium modelling by Johnson et al. (2017) of a MgO-poor composition predicts garnet-present assemblages at pressures down to ~0.7 GPa, which is lower than the compositions modelled here (0.8–1.1 GPa; Fig. 3). Therefore, a range of Sr/Y and La_N/Yb_N ratios could be expected in melts produced along a 1000 °C/GPa thermal gradient, although modal proportions of garnet in the source would likely be too low to impart a high pressure signature to the melt.

The modelled melt compositions from the 500 °C/GPa and 750 °C/GPa gradients suggest that distinguishing TTGs derived from melting at medium or high pressure may not be straightforward. Although Sr/Y and La_N/Yb_N generally increase with increasing pressure along these thermal gradients, the influence of temperature on garnet modal proportions in the residue also plays a role. Along the linear *P–T* gradients modelled here, garnet modal proportions decrease with increasing *P–T* beyond 900 °C–950 °C (Fig. 3), suggesting that higher pressures of melting cannot be always equated with higher proportions of garnet. Fractionation of Y and Yb from the system by sequestration in garnet cores could produce melt with Sr/Y and La_N/Yb_N consistent with the high pressure group of Moyen (2011) at moderate pressures and high temperatures. For instance, the modelled melts from DAT and EAT are predicted to have Sr/Y > 300 at ~1.4 GPa at > 1000 °C, corresponding to a depth of ~47 km assuming a crustal density of 3000 kg/m^3 (Fig. 8g and h; Supplementary Table 2). By contrast, melts with Sr/Y > 300 are only possible for MAB in the garnet fractionation scenario at 1.9 GPa and 950 °C, or 65 km depth (Fig. 8i). Notably, MAB also produces melts that are the least consistent with natural TTGs in terms of normative feldspar composition, suggesting that this bulk composition may not be representative of typical TTG source rocks. Presumably, basalt compositions that may stabilize greater proportions of garnet, such as that modelled by Johnson et al. (2017), would be capable of producing melts with elevated Sr/Y and La_N/Yb_N at lower pressures than those modelled here considering garnet fractionation. The bulk composition of the melting metabasite evidently exerts a first order control on Sr/Y and La_N/Yb_N of the melt produced, and as this variable is typically unknown when investigating natural TTGs, this introduces uncertainty in assigning pressures or depths of melting to TTGs based on these geochemical characteristics. Similarly, we show that Nb and Ta concentrations of the melt are influenced by the concentrations of these elements in the source, with the potential to obscure the effect of Nb and Ta partitioning between melt and rutile at high pressure. Therefore, using these geochemical characteristics of TTGs to determine the depth of melting, and therefore their geodynamic setting, should be done with caution, and only in conjunction with other geological evidence.

The results of our modelling are consistent with the conclusions of Johnson et al. (2019) regarding the link between secular change in TTG compositions and the onset of plate tectonics on Earth. Based on their compilation of TTG geochemical data, Johnson et al. (2019) found that maximum Sr/Y and La_N/Yb_N values became greater with decreasing age, consistent with these rocks recording melting at greater depths due to the

emergence of subduction with secular cooling of the mantle. Similarly, our modelling suggests that melting along a high dT/dP gradient, represented by 1000 °C/GPa, cannot reproduce this trend. Only the lower dT/dP gradients used in our modelling, 750 °C/GPa and 500 °C/GPa, can produce the higher maximum Sr/Y and La_N/Yb_N found in younger TTGs, supporting the interpretation that these rocks could only be formed after cooling of the mantle allowed for melting of metabasites at greater depths, potentially by subduction.

5. Conclusions

Thermodynamic modelling of three Archean basalt compositions was coupled with trace element modelling to evaluate the effect of open system processes during melting and source bulk composition on the Sr, Y, La, Yb, Nb, and Ta systematics of TTGs. The selected source compositions produce melts with a geochemical resemblance to natural TTGs in terms of normative feldspar composition, though many modelled melts of the MgO-enriched composition, MAB, are inconsistent with the natural record. Trace element modelling of melts from all sources produce trace element compositions consistent with TTGs that vary with source bulk composition and closed vs. open system behaviour. Concentrations of Sr, Y, La, Yb, Nb, and Ta in the melt reflect both the enrichment of these elements in the source and the stability fields and modal proportions of garnet, plagioclase, and rutile. The expected trends were observed: with increasing P–T, increasing proportions of garnet and rutile cause the concentrations of Y, Yb, Nb, and Ta to decrease in the melt, and decreasing proportions of plagioclase cause the concentration of Sr to increase in the melt. Consequently, Sr/Y and La_N/Yb_N generally increase with increasing P–T and show minor variations across the source compositions. The concentrations of Nb and Ta in the melt decrease with increasing rutile proportions but are also strongly controlled by the concentrations of Nb and Ta in the source. In the models, melt loss during anatexis has a relatively minor effect on melt trace element composition in comparison to garnet fractionation. In the latter scenario, Y and Yb are isolated from the melt, resulting in higher Sr/Y and La_N/Yb_N ratios relative to the other modelled scenarios. This allows the modelled melts to replicate the highest Sr/Y ratios of natural TTGs, which represent the high pressure TTG group as defined by Moyen (2011). These high Sr/Y and La_N/Yb_N melts are produced at a range of P and T, rather than being restricted to $P \geq 2.0$ GPa (cf. Moyen, 2011).

The results of the modelling imply that geochemical parameters of TTGs commonly used as proxies for the pressure of melting may be sensitive to factors other than pressure, including the temperature of melting and the composition of the source, particularly with garnet fractionation. This, in turn, complicates the link between the composition of TTGs and their geodynamic setting, particularly when distinguishing 'medium pressure' and 'high pressure' melting. The trace element compositions of TTGs have traditionally been a key factor in determining the geodynamic processes that produced and reworked Archean continental crust. However, using this information in isolation may be misleading, and a suite of geological evidence should be considered before reaching a conclusion.

Declaration of competing interest

The authors declare that they have no known competing financial interests or personal relationships that could have appeared to influence the work reported in this paper.

Acknowledgments

This research was funded by a National Sciences and Engineering Research Council of Canada Discovery grant to CY, and JK was supported by a Vanier Canada Graduate Scholarship. This work was completed as part of the PhD dissertation of JK and benefitted from discussions with Richard Palin, Michael Brown, and Jean-François Moyen. We thank reviewers Matthew Mayne and Richard White for their comments and suggestions, which helped to improve the clarity of the manuscript, and Associate Editor Richard Palin for editorial handling.

Appendix A. Supplementary data

Supplementary data to this article can be found online at https://doi.org/10.1016/j.gsf.2019.12.001.

References

Abbott, D., Drury, R., Smith, W.H.F., 1994. Flat to steep transition in subduction style. Geology 22, 937–940. https://doi.org/10.1130/0091-7613(1994)022<0937:FTSTIS>2.3.CO;2.

Spear, F.S., Kohn, M.J., 1996. Trace element zoning in garnet as a monitor of crustal melting. Geology 24, 1099–1102. https://doi.org/10.1130/0091-7613(1996)024<1099:TEZIGA>2.3.CO;2.

Barker, F., 1979. Trondhjemite: definition, environment and hypotheses of origin. In: Barker, F. (Ed.), Trondhjemites, Dacites, and Related Rocks, Developments in Petrology. Elsevier, Amsterdam, pp. 1–12, 6.

Bédard, J.H., 2006. A catalytic delamination-driven model for coupled genesis of Archaean crust and sub-continental lithospheric mantle. Geochem. Cosmochim. Acta 70, 1188–1214. https://doi.org/10.1016/j.gca.2005.11.008.

Bédard, J.H., 2018. Stagnant lids and mantle overturns: implications for Archaean tectonics, magmagenesis, crustal growth, mantle evolution, and the start of plate tectonics. Geosci. Front. 9, 19–49. https://doi.org/10.1016/j.gsf.2017.01.005.

Bédard, J.H., Harris, L.B., Thurston, P.C., 2013. The hunting of the snArc. Precambrian Res. 229, 20–48. https://doi.org/10.1007/s00145-016-9241-9.

Blundy, J., Wood, B., 2003. Partitioning of trace elements between crystals and melts. Earth Planet. Sci. Lett. 210, 383–397. https://doi.org/10.1016/S0012-821X(03)00129-8.

Boger, S.D., White, R.W., Schulte, B., 2012. The importance of iron speciation (Fe^{+2}/Fe^{+3}) in determining mineral assemblages: an example from the high-grade aluminous metapelites of southeastern Madagascar. J. Metamorph. Geol. 30, 997–1018. https://doi.org/10.1111/jmg.12001.

Brown, M., 2013. Granite: from genesis to emplacement. GSA Bull. 125, 1079–1113. https://doi.org/10.1130/B30877.1.

Brown, M., Johnson, T., 2018. Secular change in metamorphism and the onset of global plate tectonics. Am. Mineral. 103, 181–196. https://doi.org/10.2138/am-2018-6166.

Carlson, W.D., 2006. Rates of Fe, Mg, Mn, and Ca diffusion in garnet. Am. Mineral. 91, 1–11. https://doi.org/10.2138/am.2006.2043.

Carlson, W.D., 2012. Rates and mechanism of Y, REE, and Cr diffusion in garnet. Am. Mineral. 97, 1598–1618. https://doi.org/10.2138/am.2012.4108.

Clemens, J.D., 2015. Magmatic life at low Reynolds number: Comment. Geology 43, e357. https://doi.org/10.1130/G36512C.1.

Clemens, J.D., Helps, P.A., Stevens, G., 2009. Chemical structure in granitic magmas - a signal from the source? Trans. R. Soc. Edinb. Earth Sci. 100, 159–172. https://doi.org/10.1017/S1755691009016053.

Condie, K.C., 1981. Archean Greenstone Belts. Developments in Precambrian Geology, vol. 3. Elsevier, New York.

Condie, K.C., 1985. Secular variation in the composition of basalts: an index to mantle evolution. J. Petrol. 26, 545–563.

Condie, K.C., 2018. A planet in transition: the onset of plate tectonics on Earth between 3 and 2 Ga? Geosci. Front. 9, 51–60. https://doi.org/10.1016/j.gsf.2016.09.001.

Condie, K.C., Aster, R.C., Van Hunen, J., 2016. A great thermal divergence in the mantle beginning 2.5 Ga: geochemical constraints from greenstone basalts and komatiites. Geosci. Front. 7, 543–553. https://doi.org/10.1016/j.gsf.2016.01.006.

Drummond, M.S., Defant, M.J., 1990. A model for trondhjemite-tonalite-dacite genesis and crustal growth via slab melting: Archean to modern comparisons. J. Geophys. Res. 95 (503–21), 21, 521.

Drummond, M.S., Defant, M.J., Kepezhinskas, P.K., 1996. Petrogenesis of slab-derived trondhjemite-tonalite-dacite/adakite magmas. Trans. R. Soc. Edinb. Earth Sci. 87, 205–215.

Evans, T.P., 2004. A method for calculating effective bulk composition modification due to crystal fractionation in garnet-bearing schist: implications for isopleth thermobarometry. J. Metamorph. Geol. 22, 547–557. https://doi.org/10.1111/j.1525-1314.2004.00532.x.

Forshaw, J.B., Waters, D.J., Pattison, D.R.M., Palin, R.M., Gopon, P., 2019. A comparison of observed and thermodynamically predicted phase equilibria and mineral compositions in mafic granulites. J. Metamorph. Geol. 37, 153–179. https://doi.org/10.1111/jmg.12454.

Gaidies, F., de Capitani, C., Abart, R., 2008. THERIA_G: a software program to numerically model prograde garnet growth. Contrib. Mineral. Petrol. 155, 657–671. https://doi.org/10.1007/s00410-007-0263-z.

Gardiner, N.J., Johnson, T.E., Kirkland, C.L., Smithies, R.H., 2018. Melting controls on the lutetium–hafnium evolution of Archaean crust. Precambrian Res. 305, 479–488. https://doi.org/10.1016/j.precamres.2017.12.026.

Gardiner, N.J., Kirkland, C.L., Hollis, J., Szilas, K., Steenfelt, A., Yakymchuk, C., Heide-Jørgensen, H., 2019. Building Mesoarchaean crust upon Eoarchaean roots: the Akia Terrane, West Greenland. Contrib. Mineral. Petrol. 174, 20. https://doi.org/10.1007/s00410-019-1554-x.

Glazner, A.F., 2014. Magmatic life at low Reynolds number. Geology 42, 935–938. https://doi.org/10.1130/G36078.1.
Green, T.H., 1995. Significance of Nb/Ta as an indicator of geochemical processes in the crust-mantle system. Chem. Geol. 120, 347–359. https://doi.org/10.1016/0009-2541(94)00145-X.
Green, E.C.R., White, R.W., Diener, J.F.A., Powell, R., Holland, T.J.B., Palin, R.M., 2016. Activity–composition relations for the calculation of partial melting equilibria in metabasic rocks. J. Metamorph. Geol. 34, 845–869. https://doi.org/10.1111/jmg.12211.
Hanson, G.N., 1978. The application of trace elements to the petrogenesis of igneous rocks of granitic composition. Earth Planet. Sci. Lett. 38, 26–43. https://doi.org/10.1016/0012-821X(78)90124-3.
Harry, D.L., Green, N.L., 1999. Slab dehydration and basalt petrogenesis in subduction systems involving very young oceanic lithosphere. Chem. Geol. 160, 309–333. https://doi.org/10.1016/S0009-2541(99)00105-9.
Hastie, A.R., Kerr, A.C., McDonald, I., Mitchell, S.F., Pearce, J.A., Wolstencroft, M., Millar, I.L., 2010. Do Cenozoic analogues support a plate tectonic origin for Earth's earliest continental crust? Geology 38, 495–498. https://doi.org/10.1130/G30778.1.
Herzberg, C., Rudnick, R., 2012. Formation of cratonic lithosphere: an integrated thermal and petrological model. Lithos 149, 4–15. https://doi.org/10.1016/j.lithos.2012.01.010.
Herzberg, C., Condie, K., Korenaga, J., 2010. Thermal history of the Earth and its petrological expression. Earth Planet. Sci. Lett. 292, 79–88. https://doi.org/10.1016/j.epsl.2010.01.022.
Holland, T., Powell, R., 2003. Activity-compositions relations for phases in petrological calculations: an asymmetric multicomponent formulation. Contrib. Mineral. Petrol. 145, 492–501. https://doi.org/10.1007/s00410-003-0464-z.
Holland, T.J.B., Powell, R., 2011. An improved and extended internally consistent thermodynamic dataset for phases of petrological interest, involving a new equation of state for solids. J. Metamorph. Geol. 29, 333–383. https://doi.org/10.1111/j.1525-1314.2010.00923.x.
Holland, T.J.B., Green, E.C.R., Powell, R., 2018. Melting of peridotites through to granites: a simple thermodynamic model in the system KNCFMASHTOCr. J. Petrol. 59, 881–900. https://doi.org/10.1093/petrology/egy048.
Hollings, P., 2002. Archean Nb-enriched basalts in the northern superior province. Lithos 64, 1–14. https://doi.org/10.1016/S0024-4937(02)00154-8.
Hollings, P., Kerrich, R., 2000. An Archean arc basalt-Nb-enriched basalt-adakite association: the 2.7 Ga Confederation assemblage of the Birch-Uchi greenstone belt, Superior Province. Contrib. Mineral. Petrol. 139, 208–226. https://doi.org/10.1007/PL00007672.
Holness, M.B., Sawyer, E.W., 2008. On the pseudomorphing of melt-filled pores during the crystallization of migmatites. J. Petrol. 49, 1343–1363. https://doi.org/10.1093/petrology/egn028.
Jahn, B.-M., Glikson, A.Y., Peucat, J.J., Hickman, A.H., 1981. REE geochemistry and isotopic data of Archean silicic volcanics and granitoids from the Pilbara Block, Western Australia: implications for the early crustal evolution. Geochem. Cosmochim. Acta 45, 1633–1652. https://doi.org/10.1016/S0016-7037(81)80002-6.
Janoušek, V., Moyen, J.-F., 2019. Whole-rock Geochemical Modelling of Granite Genesis – the Current State of Play. Geological Society, London, Special Publications ,491. https://doi.org/10.1144/SP491-2018-160.
Johnson, T.E., Brown, M., Gardiner, N.J., Kirkland, C.L., Smithies, R.H., 2017. Earth's first stable continents did not form by subduction. Nature 543, 239–242. https://doi.org/10.1038/nature21383.
Johnson, T.E., Brown, M., Kaus, B.J.P., VanTongeren, J.A., 2014. Delamination and recycling of Archaean crust caused by gravitational instabilities. Nat. Geosci. 7, 47–52. https://doi.org/10.1038/ngeo2019.
Johnson, T.E., Kirkland, C.L., Gardiner, N.J., Brown, M., Smithies, R.H., Santosh, M., 2019. Secular change in TTG compositions: implications for the evolution of Archaean geodynamics. Earth Planet. Sci. Lett. 505, 65–75. https://doi.org/10.1016/j.epsl.2018.10.022.
Kelly, N.M., Harley, S.L., 2005. An integrated microtextural and chemical approach to zircon geochronology: refining the Archaean history of the Napier Complex, east Antarctica. Contrib. Mineral. Petrol. 149, 57–84. https://doi.org/10.1007/s00410-004-0635-6.
Lanari, P., Duesterhoeft, E., 2019. Modeling metamorphic rocks using equilibrium thermodynamics and internally consistent databases: past achievements, problems and perspectives. J. Petrol. 60, 19–56. https://doi.org/10.1093/petrology/egy105.
Lanari, P., Engi, M., 2017. Local bulk composition effects on metamorphic mineral assemblages. Rev. Mineral. Geochem. 83, 55–102. https://doi.org/10.2138/rmg.2017.83.3.
Martin, H., 1986. Effect of steeper Archean geothermal gradient on geochemistry of subduction-zone magmas. Geology 14, 753–756. https://doi.org/10.1130/0091-7613(1986)14<753.
Martin, H., Smithies, R.H., Rapp, R., Moyen, J.-F., Champion, D., 2005. An overview of adakite, tonalite–trondhjemite–granodiorite (TTG), and sanukitoid: relationships and some implications for crustal evolution. Lithos 79, 1–24. https://doi.org/10.1016/j.lithos.2004.04.048.
Martin, H., Moyen, J.-F., Guitreau, M., Blichert-Toft, J., Le Pennec, J.-L., 2014. Why Archaean TTG cannot be generated by MORB melting in subduction zones. Lithos 198–199, 1–13. https://doi.org/10.1016/j.lithos.2014.02.017.
Mayne, M.J., Moyen, J.-F., Stevens, G., Kaislaniemi, L., 2016. Rcrust: a tool for calculating path-dependent open system processes and application to melt loss. J. Metamorph. Geol. 34, 663–682. https://doi.org/10.1111/jmg.12199.
Mayne, M.J., Stevens, G., Moyen, J.-F., 2019. A phase equilibrium investigation of selected source controls on the composition of melt batches generated by sequential melting of an average metapelite. Geological Society, London, Special Publications 491.
Moser, D.E., Bowman, J.R., Wooden, J., Valley, J.W., Mazdab, F., Kita, N., 2008. Creation of a continent recorded in zircon zoning. Geology 36, 239–242. https://doi.org/10.1130/G24416A.1.
Moyen, J.-F., 2011. The composite Archaean grey gneisses: petrological significance, and evidence for a non-unique tectonic setting for Archaean crustal growth. Lithos 123, 21–36. https://doi.org/10.1016/j.lithos.2010.09.015.
Moyen, J.-F., Laurent, O., 2018. Archaean tectonic systems: a view from igneous rocks. Lithos 302 (303), 99–125. https://doi.org/10.1016/j.lithos.2017.11.038.
Moyen, J.-F., Martin, H., 2012. Forty years of TTG research. Lithos 148, 312–336. https://doi.org/10.1016/j.lithos.2012.06.010.
Moyen, J.-F., Stevens, G., 2006. Experimental constraints on TTG petrogenesis: implications for Archean geodynamics. In: Benn, K., Mareschal, J.-C., Condie, K.C. (Eds.), Archean Geodynamics and Environments. AGU, pp. 149–178.
Moyen, J.-F., Champion, D., Smithies, R.H., 2009. The geochemistry of Archaean plagioclase-rich granites as a marker of source enrichment and depth of melting. Trans. R. Soc. Edinb. Earth Sci. 100, 35–50. https://doi.org/10.1017/S1755691009016132.
Nagel, T.J., Hoffmann, J.E., Münker, C., 2012. Generation of Eoarchean tonalite-trondhjemite-granodiorite series from thickened mafic arc crust. Geology 40, 375–378. https://doi.org/10.1130/G32729.1.
Nicholls, I.A., Harris, K.L., 1980. Experimental rare earth element partition coefficients for garnet, clinopyroxene and amphibole coexisting with andesitic and basaltic liquids. Geochem. Cosmochim. Acta 44, 287–308. https://doi.org/10.1016/0016-7037(80)90138-6.
Otamendi, J.E., de la Rosa, J.D., Patino Douce, A.E., Castro, A., 2002. Rayleigh fractionation of heavy rare earths and yttrium during metamorphic garnet growth. Geology 30, 159–162. https://doi.org/10.1130/0091-7613(2002)030<0159:RFOHRE>2.0.CO;2.
O'Connor, J.T., 1965. A classification for quartz-rich igneous rocks based on feldspar ratios. U. S. Geol. Surv. Prof. Pap. 525, 79–84.
Palin, R.M., Dyck, B., 2018. Metamorphic consequences of secular changes in oceanic crust composition and implications for uniformitarianism in the geological record. Geosci. Front. 9, 1009–1019. https://doi.org/10.1016/j.gsf.2018.04.004.
Palin, R.M., Weller, O.M., Waters, D.J., Dyck, B., 2016a. Quantifying geological uncertainty in metamorphic phase equilibria modelling; a Monte Carlo assessment and implications for tectonic interpretations. Geosci. Front. 7, 591–607. https://doi.org/10.1016/j.gsf.2015.08.005.
Palin, R.M., White, R.W., Green, E.C.R., 2016b. Partial melting of metabasic rocks and the generation of tonalitic–trondhjemitic–granodioritic (TTG) crust in the Archaean: constraints from phase equilibrium modelling. Precambrian Res. 287, 73–90. https://doi.org/10.1016/j.precamres.2016.11.001.
Pichavant, M., Montel, J.-M., Richard, L.R., 1992. Apatite solubility in peraluminous liquids: experimental data and an extension of the Harrison-Watson model. Geochem. Cosmochim. Acta 56, 3855–3861. https://doi.org/10.1016/0016-7037(92)90178-L.
Polat, A., Kerrich, R., 2001. Magnesian andesites, Nb-enriched basalt-andesites, and adakites from late-Archean 2.7 Ga Wawa greenstone belts, Superior Province, Canada: implications for late Archean subduction zone petrogenetic processes. Contrib. Mineral. Petrol. 141, 36–52. https://doi.org/10.1007/s004100000223.
Powell, R., Holland, T.J.B., 1988. An internally consistent dataset with uncertainties and correlations: 3. Applications to geobarometry, worked examples and a computer program. J. Metamorph. Geol. 6, 173–204. https://doi.org/10.1111/j.1525-1314.1988.tb00415.x.
Powell, R., Holland, T.J.B., 2008. On thermobarometry. J. Metamorph. Geol. 26, 155–179. https://doi.org/10.1111/j.1525-1314.2007.00756.x.
Presnall, D.C., 1969. The geometrical analysis of partial fusion. Am. J. Sci. 267, 1178–1194.
Pyle, J.M., Spear, F.S., 1999. Yttrium zoning in garnet: coupling of major and accessory phases during metamorphic reactions. Geol. Mater. Res. 1, 1–49.
Qian, Q., Hermann, J., 2013. Partial melting of lower crust at 10-15 kbar: constraints on adakite and TTG formation. Contrib. Mineral. Petrol. 165, 1195–1224. https://doi.org/10.1007/s00410-013-0854-9.
Rapp, R.P., Watson, E.B., 1995. Dehydration melting of metabasalt at 8–32 kbar: implications for continental growth and crust-mantle recycling. J. Petrol. 36, 891–931.
Rapp, R.P., Watson, E.B., Miller, C.F., 1991. Partial melting of amphibolite/eclogite and the origin of Archean trondhjemites and tonalites. Precambrian Res. 51, 1–25.
Reichardt, H., Weinberg, R.F., 2012. Hornblende chemistry in meta- and diatexites and its retention in the source of leucogranites: an example from the Karakoram Shear Zone, NW India. J. Petrol. 53, 1287–1318. https://doi.org/10.1093/petrology/egs017.
Rosenberg, C.L., Handy, M.R., 2005. Experimental deformation of partially melted granite revisited: implications for the continental crust. J. Metamorph. Geol. 23, 19–28. https://doi.org/10.1111/j.1525-1314.2005.00555.x.
Ryerson, F.J., Watson, E.B., 1987. Rutile saturation in magmas: implications for Ti-Nb-Ta depletion in island-arc basalts. Earth Planet. Sci. Lett. 86, 225–239.
Sawyer, E.W., 1999. Criteria for the recognition of partial melting. Phys. Chem. Earth 24, 269–279. https://doi.org/10.1016/S1464-1895(99)00029-0.
Schmidt, M.W., Thompson, A.B., 1996. Epidote in calc-alkaline magmas: an experimental study of stability, phase relationships, and the role of epidote in magmatic evolution. Am. Mineral. 81, 462–474. https://doi.org/10.2138/am-1996-3-420.
Shaw, D.M., 1970. Trace element fractionation during anatexis. Geochem. Cosmochim. Acta 34, 237–243. https://doi.org/10.1016/0016-7037(70)90009-8.
Sizova, E., Gerya, T., Stüwe, K., Brown, M., 2015. Generation of felsic crust in the Archean: a geodynamic modeling perspective. Precambrian Res. 271, 198–224. https://doi.org/10.1016/j.precamres.2015.10.005.

Smithies, R.H., Champion, D.C., Van Kranendonk, M.J., 2009. Formation of Paleoarchean continental crust through infracrustal melting of enriched basalt. Earth Planet. Sci. Lett. 281, 298–306. https://doi.org/10.1016/j.epsl.2009.03.003.

Smithies, R.H., Ivanic, T.J., Lowrey, J.R., Morris, P.A., Barnes, S.J., Wyche, S., Lu, Y.J., 2018. Two distinct origins for Archean greenstone belts. Earth Planet. Sci. Lett. 487, 106–116. https://doi.org/10.1016/j.epsl.2018.01.034.

Springer, W., Seck, H.A., 1997. Partial fusion of basic granulites at 5 to 15 kbar: implications for the origin of TTG magmas. Contrib. Mineral. Petrol. 127, 30–45.

Stern, C.R., Huang, W.-L., Wyllie, P.J., 1975. Basalt-andesite-rhyolite-H_2O: crystallization intervals with excess H_2O and H_2O-undersaturated liquidus surfaces to 35 kilobars, with implications for magma genesis. Earth Planet. Sci. Lett. 28, 189–196. https://doi.org/10.1016/0012-821X(75)90226-5.

Stevens, G., Villaros, A., Moyen, J.-F., 2007. Selective peritectic garnet entertainment as the origin of geochemical diversity in S-type granites. Geology 35, 9–12. https://doi.org/10.1130/G22959A.1.

Stuck, T.J., Diener, J.F.A., 2018. Mineral equilibria constraints on open-system melting in metamafic compositions. J. Metamorph. Geol. 36, 255–281. https://doi.org/10.1111/jmg.12292.

Szilas, K., Van Hinsberg, V.J., Kisters, A.F.M., Hoffmann, J.E., Windley, B.F., Kokfelt, T.F., Scherstén, A., Frei, R., Rosing, M.T., Münker, C., 2013. Remnants of Arc-related Mesoarchaean oceanic crust in the Tartoq group of SW Greenland. Gondwana Res. 23, 436–451. https://doi.org/10.1016/j.gr.2011.11.006.

Taylor, J., Stevens, G., 2010. Selective entrainment of peritectic garnet into S-type granitic magmas: evidence from Archaean mid-crustal anatectites. Lithos 120, 277–292. https://doi.org/10.1016/j.lithos.2010.08.015.

Villaros, A., Laurent, O., Couzinié, S., Moyen, J.-F., Mintrone, M., 2018. Plutons and domes: the consequences of anatectic magma extraction—example from the southeastern French Massif Central. Int. J. Earth Sci. 107, 2819–2842. https://doi.org/10.1007/s00531-018-1630-x.

Watson, E.B., Capobianco, C.J., 1981. Phosphorus and the rare earth elements in felsic magmas: an assessment of the role of apatite. Geochem. Cosmochim. Acta 45, 2349–2358.

Watson, E.B., Vicenzi, E.P., Rapp, R.P., 1989. Inclusion/host relations involving accessory minerals in high-grade metamorphic and anatectic rocks. Contrib. Mineral. Petrol. 101, 220–231. https://doi.org/10.1007/BF00375308.

White, R.W., Powell, R., 2002. Melt loss and the preservation of granulite facies mineral assemblages. J. Metamorph. Geol. 20, 621–632. https://doi.org/10.1046/j.1525-1314.2002.00206.x.

White, R.W., Powell, R., Halpin, J.A., 2004. Spatially-focussed melt formation in aluminous metapelites from Broken Hill, Australia. J. Metamorph. Geol. 22, 825–845. https://doi.org/10.1111/j.1525-1314.2004.00553.x.

White, R.W., Pomroy, N.E., Powell, R., 2005. An in situ metatexite-diatexite transition in upper amphibolite facies rocks from Broken Hill, Australia. J. Metamorph. Geol. 23, 579–602. https://doi.org/10.1111/j.1525-1314.2005.00597.x.

White, R.W., Powell, R., Holland, T.J.B., Johnson, T.E., Green, E.C.R., 2014. New mineral activity-composition relations for thermodynamic calculations in metapelitic systems. J. Metamorph. Geol. 32, 261–286. https://doi.org/10.1111/jmg.12071.

White, R.W., Palin, R.M., Green, E.C.R., 2017. High-grade metamorphism and partial melting in Archean composite grey gneiss complexes. J. Metamorph. Geol. 35, 181–195. https://doi.org/10.1111/jmg.12227.

Wickham, H., 2011. ggplot2, vol. 3. Wiley Interdisciplinary Reviews: Computational Statistics, pp. 180–185. https://doi.org/10.1002/wics.147.

Wyman, D.A., Ayer, J.A., Devaney, J.R., 2000. Niobium-enriched basalts from the Wabigoon subprovince, Canada: evidence for adakitic metasomatism above an Archean subduction zone. Earth Planet. Sci. Lett. 179, 21–30. https://doi.org/10.1016/S0012-821X(00)00106-0.

Yakymchuk, C., Brown, M., 2014. Consequences of open-system melting in tectonics. J. Geol. Soc. 171, 21–40. https://doi.org/10.1144/jgs2013-039.

Yakymchuk, C., Brown, M., 2019. Divergent behaviour of Th and U during anatexis: implications for the thermal evolution of orogenic crust. J. Metamorph. Geol. 37, 899–916. https://doi.org/10.1111/jmg.12469.

Yakymchuk, C., Zhao, W., Wan, Y., Lin, S., Longstaffe, F.J., 2019. Fluid-present anatexis of Neoarchean tonalite and amphibolite in the western Shandong province. Lithos 326–327, 110–124. https://doi.org/10.1016/j.lithos.2018.12.014.